

Amortized Variational Transdimensional Inference

Laurence Davies^{1*} Dan Mackinlay^{2^} Rafael Oliveira^{2^} Scott A. Sisson^{1§}

¹University of New South Wales ²CSIRO Data61

*laurence@latentlogic.com.au, §scott.sisson@unsw.edu.au

^ {dan.mackinlay,rafael.dossantosdeoliveira}@data61.csiro.au

Abstract

The expressiveness of flow-based models combined with stochastic variational inference (SVI) has, in recent years, expanded the application of optimization-based Bayesian inference to include problems with complex data relationships. However, until now, SVI using flow-based models has been limited to problems of fixed dimension. We introduce CoSMIC normalizing flows (COntextually-Specified Masking for Identity-mapped Components), an extension to neural autoregressive conditional normalizing flow architectures that enables using a single amortized variational density for inference over a transdimensional target distribution. We propose a combined stochastic variational transdimensional inference (VTI) approach to training CoSMIC flows using techniques from Bayesian optimization and Monte Carlo gradient estimation. Numerical experiments demonstrate the performance of VTI on challenging problems that scale to high-cardinality model spaces.

1 Introduction

Amortized variational inference (8) is a universal topic in statistics and machine learning that has seen a surge in interest since the introduction of normalizing flows (36). An amortized density function can be used for a variety of downstream tasks, such as importance sampling (36), simulation-based inference (32; 48), adaptive MCMC (13), and generative modeling (23). While many existing approaches only consider continuous supports, there is a growing interest in applications where the support is either discrete or discretely indexed (9). One such application concerns a *target* transdimensional probability distribution π with support

$$\mathcal{X} = \bigcup_{m \in \mathcal{M}} (\{m\} \times \Theta_m), \quad (1)$$

where \mathcal{M} is a finite discrete *index* set, $\Theta_m \subseteq \mathbb{R}^{d_m}$, and where the dimension d_m of Θ_m may vary with m . Hence \mathcal{X} is a *transdimensional* space (17; 40). Such spaces arise naturally in Bayesian model inference, where the sets Θ_m correspond to model *parameters*, and $m \in \mathcal{M}$ is a *model index*. Model indices can parameterize various practical inference problems, such as variable selection, mixtures-of-regressions, or learning directed acyclic graphs (DAGs) from data.

This article is concerned with estimating the target distribution π with associated density function $\pi(m, \theta_m)$, $\theta_m \in \Theta_m$, which varies in dimension depending on m . (Note that for simplicity we refer to $\pi(m, \theta_m)$ and related functions as *density* functions, even though they are not continuous.) Typically, this density is only available in a conditional unnormalized form, $\eta(\theta_m | m) = \mathcal{Z}_m \pi(\theta_m | m)$, where $\mathcal{Z}_m = \int_{\Theta_m} \eta(\theta_m | m) d\theta_m$. The factorization $\eta(m, \theta_m) = \eta(\theta_m | m) \pi(m)$ implies there is a discrete target probability mass function over models, $\pi(m) = \mathcal{Z}_m \mathcal{Z}^{-1}$, where $\mathcal{Z} = \sum_{m \in \mathcal{M}} \mathcal{Z}_m$. Estimation of $\eta(m, \theta_m)$ then becomes estimation of both $\eta(\theta_m | m)$ and $\pi(m)$.

In the presence of a likelihood function $p(\mathcal{D} | m, \theta_m)$ for data \mathcal{D} , and priors $p(\theta_m | m)$ and $p(m)$, the target distribution is defined by the \mathcal{D} -conditional transdimensional posterior $\pi(m, \theta_m | \mathcal{D}) \propto p(\mathcal{D} | m, \theta_m)p(\theta_m|m)p(m)$. In the context of *variational Bayesian inference* (20; 2), the process by which a variational approximation of the transdimensional posterior $\pi(m, \theta_m | \mathcal{D})$ can be constructed has not been addressed in generality. Such a scheme would approximate some unnormalized target density $\eta(m, \theta_m | \mathcal{D}) = \mathcal{Z}\pi(m, \theta_m | \mathcal{D})$ by optimizing over the parameters $\phi \in \mathbb{R}^{n_\phi}$, $\psi \in \mathbb{R}^{n_\psi}$ of a tractable variational density family $q_{\psi, \phi}(m, \theta_m) = q_\phi(\theta_m | m)q_\psi(m)$ via an objective function

$$\psi^*, \phi^* := \arg \min_{\psi, \phi} \mathcal{L}(\psi, \phi), \quad \mathcal{L}(\psi, \phi) = D_{\text{KL}}(q_{\psi, \phi} || \pi) \quad (2)$$

where the loss \mathcal{L} is the Kullback-Leibler (KL) divergence. There are two immediate impediments to constructing such a variational approximation. The first is defining and optimizing q_ϕ as θ_m may vary in dimension conditional on m . The second is the inference of q_ψ for discrete latent variables m during the optimization of q_ϕ , which amounts to optimization over non-stationary rewards as the convergence of $\phi \rightarrow \phi^*$ and $\psi \rightarrow \psi^*$ are interdependent.

Background: Flow-based models for stochastic variational inference: Rezende and Mohamed (36) showed that a *normalizing flow* for q_ϕ (with fixed m) is able to approximate many challenging fixed-dimensional distributions that are not well approximated by common parametric families. By construction, a normalizing flow is defined by a diffeomorphism $T_\phi : \mathbb{R}^d \rightarrow \mathbb{R}^d$ between two random vectors $\theta \sim q$ and $z \sim \nu_d$, such that their distributions q and ν_d are absolutely continuous with respect to a d -dimensional Lebesgue measure, have well-defined densities $q(\theta)$ and $\nu_d(z)$ respectively, and can be related by a change of variables $z = T_\phi(\theta)$ so that $q(\theta; \phi) = \nu_d(T_\phi(\theta)) |\det \nabla T_\phi(\theta)|$, $\theta \in \mathbb{R}^d$. For typical normalizing flow-based models, we refer to ν_d as the *reference* distribution and assume it factorizes into a product of d identical marginal distributions $\nu_d = \nu \otimes \dots \otimes \nu = \otimes_d \nu$. Construction of T_ϕ is typically achieved by defining d bijective, univariate functions $\tau_{\rho_i} : \mathbb{R} \mapsto \mathbb{R}$, $z_i = \tau_{\rho_i}(\theta_i)$ for $i \in \{1, \dots, d\}$. The parameters $\rho_i = \text{NN}_\phi(\theta_{\setminus i})$ for the i^{th} transformation are determined by a neural network NN_ϕ such that ρ_i is not dependent on θ_i , so that the inverse $\tau_{\rho_i}^{-1}(\cdot)$ can therefore be calculated without requiring NN_ϕ^{-1} . This dependency restriction is upheld if the neural network NN_ϕ is constructed to be *autoregressive* with respect to the inputs $\theta_1, \dots, \theta_d$ (31). The autoregressive nature of NN_ϕ is crucial to the results in Section 2. A *conditional* normalizing flow is a natural extension of a normalizing flow whereby a conditioning variate, ξ , is passed as a contextual input to NN_ϕ , such that $\rho_i = \text{NN}_\phi(\theta_{\setminus i}; \xi)$. Typical applications include classification, where ξ is an index, or likelihood estimation (47) where ξ encodes the parameters of the likelihood function.

The MADE autoregressive encoder (15) enabled autoregressive neural flow architectures, which can be coupled with any τ such as affine (31) and spline (11) based transformations. The computational complexity of the autoregressive flow is direction-dependent, being sequentially $O(d)$ in the inverse direction when compared with the forward direction. The inverse autoregressive flow (IAF) (22) avoids the sequential computational complexity in the variational setting by setting $\theta = T_\phi(z)$, yielding the variational density $q_\phi(\theta_m) = \nu_d(T_\phi^{-1}(\theta)) |\det \nabla T_\phi^{-1}(\theta)| = \nu_d(z) |\det \nabla T_\phi(z)|^{-1}$.

Contributions: In this article, we introduce CoSMIC (*C*ontextually-Specified Masking for Identity-mapped Component) flows, a widely applicable and simple modification to conditional neural flow architectures (Section 2). CoSMIC flows fundamentally expand the use cases for normalizing flows to encompass amortized variational inference applications so that a single amortized variational density can be used for inference over a transdimensional target distribution. In Section 3, we demonstrate the efficacy of CoSMIC transformations within a novel *variational transdimensional inference* (VTI) framework with two implementations. The first builds upon principles of Bayesian optimization (42), and the second uses Monte Carlo gradient estimation (28). We also provide a theoretical analysis of VTI approximation error bounds under a Gaussian process surrogate, and convergence guarantees for the marginal model distribution under convergent optimization steps. Finally, we demonstrate the applicability of VTI to problems with model spaces that cannot be easily enumerated within the memory limitations of current computing architectures. In particular, Section 5 explores problems in Bayesian robust variable selection (29) and Bayesian model discovery of directed acyclic graphs (18) (DAGs). Python/Pytorch CUDA code for all experiments will be made available at <https://github.com/daviesl/avti>.

2 Formulating a transdimensional variational density

Rather than constructing a variational density separately for each model $m \in \mathcal{M}$, it is preferable to construct a single density on the transdimensional support \mathcal{X} . To account for the varying dimension of θ_m , we adopt the *dimension saturation* approach of Brooks et al. (5), where the dimension of the parameter space conditional on each model is unified across all models. This is achieved by augmenting the space of model-conditional parameters with auxiliary variables $\mathbf{u} \sim \nu$, as discussed below. We use the notation $\setminus m$ to identify auxiliary variables of dimension $d_{\max} - d_m$, where $d_{\max} := \max_m \{d_m\}$. We define the saturated support to be $(\theta_m, \mathbf{u}_{\setminus m}) \in \Theta_m \times \mathcal{U}_m \subseteq \mathbb{R}^{d_{\max}}$, with an associated unnormalized, dimension-saturated conditional target density

$$\tilde{\eta}(\theta_m, \mathbf{u}_{\setminus m} | m) = \eta(\theta_m | m) \nu_{\setminus m}(\mathbf{u}_{\setminus m}). \quad (3)$$

Defined on the same augmented support is the family of saturated variational densities

$$\tilde{q}_{\psi, \phi}(m, \theta_m, \mathbf{u}_{\setminus m}) = \tilde{q}_{\phi}(\theta_m, \mathbf{u}_{\setminus m} | m) q_{\psi}(m), \quad (4)$$

where, noting the availability of a transport $(\theta_m, \mathbf{u}_{\setminus m}) = T_{\phi}(z | m)$, $z \in \mathcal{U}^{d_{\max}}$, we define the IAF

$$\begin{aligned} \tilde{q}_{\phi}(\theta_m, \mathbf{u}_{\setminus m} | m) &:= \nu_{d_{\max}}(T_{\phi}^{-1}(\theta_m, \mathbf{u}_{\setminus m} | m)) \left| \det \nabla T_{\phi}^{-1}(\theta_m, \mathbf{u}_{\setminus m} | m) \right|, \\ &= \nu_{d_{\max}}(z) \left| \det \nabla T_{\phi}(z | m) \right|^{-1}. \end{aligned} \quad (5)$$

The goal is to show that equation 5 factorizes into an active part and an *i.i.d.* auxiliary part, i.e.

$$\tilde{q}_{\phi}(\theta_m, \mathbf{u}_{\setminus m} | m) = q_{\phi}(\theta_m | m) \nu_{d_{\setminus m}}(\mathbf{u}_{\setminus m}), \quad (6)$$

and to exploit this factorization in the construction of a transdimensional loss function. To achieve this factorization, we define the following notation. Let $A_i : \mathcal{M} \rightarrow \{0, 1\}$ flag whether latent coordinate i appears in model m , and let $B_i : \{0, 1\} \rightarrow \{0, 1\}^{|\rho_i|}$, $B_i(b) = (b, \dots, b)$, broadcast this bit to the corresponding parameter block. Their composition $C_i := B_i \circ A_i : \mathcal{M} \rightarrow \{0, 1\}^{|\rho_i|}$ therefore activates *exactly* the autoregressive parameters ρ_i needed by $\tau_{\rho_i}(z^{(i)})$ under model m . Concatenating the blocks gives the global context-to-mask map (see Figure 1(b) for a visualization):

$$C(m) := (C_1(m), \dots, C_{d_{\max}}(m)) \in \{0, 1\}^{|\rho|}, \quad |\rho| = \sum_{i=1}^{d_{\max}} |\rho_i|. \quad (7)$$

Similarly, A and B denote the respective coordinate-concatenated maps similar in form to equation 7. After a fixed left–right permutation aligning latents with θ_m , Proposition 2.2 proves this factorization is *exact* for any autoregressive network NN_{ϕ} that parametrizes the transport T_{ϕ} .

Recalling the univariate bijective maps of the inverse autoregressive flow as $\tau_{\rho_i} : \mathbb{R} \mapsto \Theta_i$ for $i = 1, \dots, d_{\max}$, we assume the existence of a *static* point ρ^{Id} such that $\tau_{\rho^{\text{Id}}}(z) = z$ for all $z \in \mathbb{R}$, i.e., the transform becomes the identity map at ρ^{Id} . For example, a simple affine transformation (scale and location shift) is $\theta = \tau_{\rho_i}(z) = \rho^{(0)} + \rho^{(1)}z$, where $\rho_i = (\rho^{(0)}, \rho^{(1)})$. In this case, the static point is $\rho^{\text{Id}} = (0, 1)$ as then $\theta = z$. We can then construct simple mechanism for “choosing” between ρ_i and ρ^{Id} for each individual transform τ , $i = 1, \dots, d_{\max}$, via the convex combination

$$\rho_i^C = (\mathbf{1} - C_i(m))\rho^{\text{Id}} + C_i(m)\rho_i, \quad m \in \mathcal{M}. \quad (8)$$

Each coordinate-wise transform then becomes $\theta_m^{(i)} = \tau_{\rho_i^C}(z^{(i)})$, $i \in \{1, \dots, d_{\max}\}$. That is, the transformation parameters become a context-dependent composition of the elements of ρ_i and the static point ρ^{Id} (Figure 1(c)). A composition of transforms parametrized according to equation 8 is a *Context-Specified Masking for Identity-mapped Components (CoSMIC)* normalizing flow.

Lemma 2.1. *For a CoSMIC normalizing flow, $\mathbf{u}_{\setminus m} = \mathbf{z}_{\setminus m}$.*

Proof. Let $I(m) = \{i \in \{1, \dots, d_{\max}\} : A_i(m) = 1\}$, and I^c be the complement. The result holds from equation 8 as, for all coordinates $i \in I^c(m)$, $\mathbf{u}_{\setminus m}^{(i)} = \tau_{\rho_i^C}(z_{\setminus m}^{(i)}) = \tau_{\rho^{\text{Id}}}(z_{\setminus m}^{(i)}) = z_{\setminus m}^{(i)}$. \square

Proofs of the following Proposition 2.2 and Corollary 2.3 are in Appendix A.

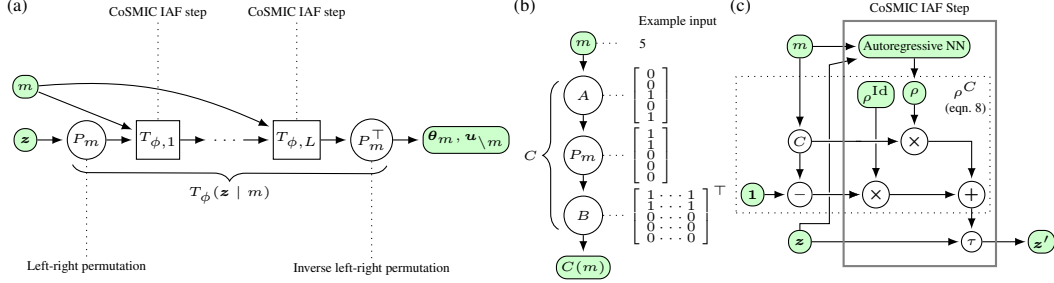


Figure 1: Overview of (a) CoSMIC flow composition, (b) Context-to-mask map, (c) A single CoSMIC IAF step.

Proposition 2.2. Fix $m \in \mathcal{M}$. Let P_m be the permutation matrix that places the coordinates indexed by $I(m)$ (from Lemma 2.1) before those in $I^c(m)$ while preserving the original order inside each group. Define the left-right-permuted flow $T_\phi^{(P_m)} := P_m^{-1} \circ T_\phi \circ P_m$ and the corresponding density $\tilde{q}_\phi^{(P_m)}(\theta_m, \mathbf{u}_{\setminus m}) = \nu_{d_{\max}}(\mathbf{z}) |\det \nabla T_\phi^{(P_m)}(\mathbf{z} | m)|^{-1}$, $\mathbf{z} = T_\phi^{(P_m), -1}(\theta_m, \mathbf{u}_{\setminus m})$. Redefine $C := C^{(P_m)} = B \circ P_m \circ A$. Then (a) $\tilde{q}_\phi^{(P_m)}(\theta_m, \mathbf{u}_{\setminus m})$ factorizes as per equation 6 with the substitution $\tilde{q}_\phi := \tilde{q}_\phi^{(P_m)}$, and (b) the marginal $q_\phi(\theta_m | m)$ is consistent.

From here on, we use the notational convenience $T_\phi := T_\phi^{(P_m)}$ and $q_\phi := q_\phi^{(P_m)}$ to denote the composition of transforms and associated variational density that include the left-right permutation P_m required by Proposition 2.2. We also write the partitioning $\mathbf{z} = (\mathbf{z}_m, \mathbf{z}_{\setminus m})$ as explicitly obtained by $[\mathbf{z}_m \mathbf{z}_{\setminus m}]^\top = P_m \mathbf{z}$. By construction, $\nu_{d_{\max}} = \nu_{d_m} \otimes \nu_{d_{\setminus m}}$, i.e. $\nu_{d_{\max}}(\mathbf{z}) = \nu_{d_m}(\mathbf{z}_m) \nu_{d_{\setminus m}}(\mathbf{z}_{\setminus m})$.

Corollary 2.3. Given Lemma 2.1 and Proposition 2.2, then

$$\frac{\nu_{d_{\max}}(\mathbf{z}) |\det \nabla T_\phi(\mathbf{z} | m)|^{-1}}{\tilde{\eta}(T_\phi(\mathbf{z} | m) | m)} = \frac{\nu_{d_m}(\mathbf{z}_m) |\det \nabla T_\phi(\mathbf{z} | m)|^{-1}}{\eta(\theta_m | m)} := h_\phi(\mathbf{z} | m), \quad (9)$$

and the loss function in equation 2 becomes

$$\mathcal{L}(\psi, \phi) = \mathbb{E}_{m \sim q_\psi} [\ell(m; \phi) - \log p(m) + \log q_\psi(m)], \quad (10)$$

where

$$\ell(m; \phi) := \mathbb{E}_{\mathbf{z} \sim \nu_{d_{\max}}} [\log h_\phi(\mathbf{z} | m)]. \quad (11)$$

The implementation of a CoSMIC inverse autoregressive flow step T_i as part of a composition of transforms $T_L \circ \dots \circ T_1$ is visualized in Figure 1(a). Individual architectures for affine and rational quadratic spline transforms (11) and compositions are described in Appendix A.2.

3 Formulating a model weights distribution

Formulating and estimating q_ψ is not as straightforward as that of q_ϕ because the discrete random variables $m \sim q_\psi$ are not automatically linked to the density parameters ψ by automatic differentiation. This problem naturally lends itself to methods developed in black-box variational inference (34; 45; 46) and multi-armed bandits (6), as described below. The representation of m is any discrete random variable on a finite space \mathcal{M} . Writing the true distribution of m as π_m , a finite \mathcal{M} implies the existence of a categorical distribution π_ζ which is bijectively equivalent to π_m . The random variables $\zeta \sim \pi_\zeta$ exist on the finite support $\zeta \in \mathcal{C} \subset \mathbb{N}$, thus $|\mathcal{C}| = |\mathcal{M}|$. This property is used by the surrogate-based approach described in Section 3.1. We formalize this concept via the following.

Proposition 3.1. Every finite discrete distribution over a finite support $\mathcal{M} = \{m_1, m_2, \dots, m_k\}$ has a unique representation as a categorical distribution. Specifically, there exists a bijective mapping between the set of all finite discrete distributions on \mathcal{M} and the set of categorical distributions parameterized by probability vectors ψ^ζ over \mathcal{M} . (Proof in Appendix C).

We consider two approaches to model q_ψ . Firstly, we derive a non-parametric surrogate-based approach which comes equipped with theoretical convergence guarantees and is applicable to model spaces \mathcal{M} of low cardinality. We then present an approach based on parametric models that can scale to arbitrarily large spaces \mathcal{M} that are trained using doubly stochastic gradient estimators.

3.1 Estimation via surrogate

The objective in Equation (10) can be rewritten as a single-variable objective with respect to ϕ :

$$\phi^* \in \arg \min_{\phi} \min_{\psi} \mathcal{L}(\psi, \phi) = \arg \max_{\phi} \max_{q_\psi \in \mathcal{P}_\Psi} \mathbb{E}_{m \sim q_\psi} [-\ell(m; \phi) + \log p(m)] + H[q_\psi], \quad (12)$$

where \mathcal{P}_Ψ denotes the space of probability measures over \mathcal{M} parameterized by $\psi \in \Psi \subseteq \mathbb{R}^{n_\psi}$, and H denotes entropy. If we replace \mathcal{P}_Ψ by $\mathcal{P}(\mathcal{M})$, i.e., the whole space of probability measures over \mathcal{M} , the solution to the inner optimization problem admits a closed-form expression:

$$q_{\ell, \phi}^*(m) := \frac{p(m) \exp(-\ell(m; \phi))}{\sum_{m' \in \mathcal{M}} p(m') \exp(-\ell(m'; \phi))}. \quad (13)$$

Computing the expression above within an optimization loop over ϕ in practice would, however, require the evaluation of flow-based densities over the entire model space. We may, instead, follow a cheaper-to-evaluate density $q_{u, \phi}$ which approximates $q_{\ell, \phi}^*$ for a given ϕ , by means of learning a surrogate model over ℓ within the *same* optimization loop¹. In particular, we derive a Gaussian process (GP) upper confidence bound (41), which provides the following approximation to the optimal model probabilities:

$$q_{u, t}(m) := \frac{p(m) \exp u_t(m)}{\sum_{m' \in \mathcal{M}} p(m') \exp u_t(m')}, \quad (14)$$

where $u_t(m) := \mu_t(m, \phi_t) + \beta \sigma_t(m, \phi_t)$, with μ_t and σ_t^2 representing the posterior mean and variance of a GP model conditioned on all mini-batches of data $\mathcal{B}_t := \{\phi_{t-1}, m_{t,i}, \log h_{\phi_{t-1}}(z_{t,i} | m_{t,i})\}_{i=1}^B$ available at iteration t of stochastic gradient descent, and ϕ_t denotes the current flow parameters. In this form, u_t provides an upper confidence bound (UCB) over $-\ell(m; \phi_t)$ determined by the choice of confidence parameter $\beta > 0$. The GP posterior mean and variance can be derived in closed form if the observation noise is Gaussian with, e.g., variance σ_ϵ^2 . We, however, show that a sub-Gaussian noise assumption is sufficient to use a conventional GP model. In addition, if ϕ_t follows a convergent sequence (e.g., by ensuring diminishing step sizes during gradient-based optimization), we provide the following guarantee.

Corollary 3.2. *Let $\ell \sim \mathcal{GP}(0, \kappa)$, where $\kappa : (\mathcal{M} \times \Phi)^2 \rightarrow \mathbb{R}$ is a bounded, continuous positive-semidefinite kernel over $\mathcal{M} \times \Phi$. Assume $\log h_\phi(z|m) - \ell(m; \phi)$ is σ_ϵ^2 -sub-Gaussian with respect to $z \sim \nu$. Then, if ϕ_t follows a convergent sequence, the following also holds:*

$$D_{\text{KL}}(q_{u, t} || q_{\ell, \phi}^*) \in \mathcal{O}_{\mathbb{P}}(t^{-1/2}), \quad (15)$$

where $\mathcal{O}_{\mathbb{P}}$ characterizes convergence in probability.²

This is a direct application of Theorem B.3, derived in the Appendix. The result above tells us that the UCB-based models distribution approaches the optimal distribution at a rate of $\mathcal{O}_{\mathbb{P}}(t^{-1/2})$ and ultimately converges to it as $t \rightarrow \infty$. Therefore, a stochastic gradient optimizer using samples from the surrogate density $q_{u, t}$ should asymptotically converge to the optimization path determined by the optimal q_{ℓ, ϕ_t}^* . That is, under appropriate settings for, e.g., its learning rate schedule, the optimization will converge to ϕ^* .

Due to the reliance on GP-based approximations, a naive implementation of this approach would incur a cost of $\mathcal{O}(B^3 t^3)$ per stochastic gradient step, where B is the mini-batch size due to the requirement of performing matrix inversions (35). However, sparse approximations to GPs can significantly reduce this cost to make it practically implementable (35; 16). In particular, for our purposes, we implemented a diagonal Gaussian approximation, which makes the cost linear in the batch size and constant in t via a mean-field approximation.

¹We are here assuming that the prior $p(m)$ is cheap to evaluate. If not, we can model $-\ell(m; \phi) + \log p(m)$, instead, with a surrogate, which leads to similar theoretical guarantees after minimal adjustments.

² $\xi_t \in \mathcal{O}_{\mathbb{P}}(g_t)$ if $\lim_{C \rightarrow \infty} \limsup_{t \rightarrow \infty} \mathbb{P}[\xi_t g_t^{-1} > C] = 0$.

3.2 Categorical and neural probability mass functions

In general, by Proposition 3.1, we may represent probability distributions over the model space \mathcal{M} arbitrarily via parametrizations of categorical distributions. A drawback of the surrogate-based approach above is the need to maintain and update estimates over the entire model space, which can be impractical for spaces of very large cardinality, as one may face with DAGs, for example. Hence, we introduce two approaches based on parametric models.

Categorical model: Assume $|\mathcal{M}| = M \in \mathbb{N}$. Then, for $\psi \in \mathbb{R}^M$, the distribution over \mathcal{M} is defined by $q_\psi(m) := (\sum_{j=1}^M \exp \psi_j)^{-1} \sum_{i=1}^M \mathbb{I}[m_i = m] \exp \psi_i$. The logit weights vector ψ is unconstrained in \mathbb{R}^M and can be jointly optimized with ϕ by gradient methods. Note that density evaluations and the entropy can be readily computed, although the memory required is $\mathcal{O}(|\mathcal{M}|)$.

Autoregressive model: If the model space is too large to keep track of a categorical weights vector, another approach is to use a more structured sample generation process which allows for the number of parameters to be smaller than the dimensionality of the space, i.e., $\dim(\psi) < M$. For instance, Germain et al. (15) proposed an autoregressive parametrization for distributions over binary strings $\mathbf{s} \in \{0, 1\}^{d_s}$ via the decomposition $p_\psi(\mathbf{s}) = \prod_{i=1}^{d_s} p_\psi(s_i | s_1, \dots, s_{i-1})$. For each \mathbf{s} , we may assign a unique $m \in \mathcal{M}$ and therefore define $q_\psi(m) := p_\psi(\mathbf{s}(m))$. The conditional densities and sampling can be implemented via MADE, allowing us to map the entire model space with fewer parameters as long as $2^{d_s} \geq |\mathcal{M}|$. The same reasoning can be applied to a DAG via decomposition of its adjacency matrix. More details are provided in Appendix F.8 with the implementation for DAGs in Appendix F.7.

3.3 Estimation via Monte Carlo gradients

When $|\mathcal{M}|$ is too large to use a surrogate-based approach, or to even parameterize an entire vector of categorical weights in physical memory, we can employ neural-based methods that use gradient descent and estimation of the gradients of ψ via Monte Carlo estimation of gradients (MCG) (28). Expressed in terms of the distribution of models and its parameters ψ , we have

$$\nabla_\psi q_\psi(m) = q_\psi(m) \nabla_\psi \log q_\psi(m). \quad (16)$$

The gradient of the expectation in equation 10 with respect to ψ is

$$\nabla_\psi \mathcal{L}(\psi, \phi) = \mathbb{E}_{m \sim q_\psi} [\ell(m; \phi) \nabla_\psi \log q_\psi(m)] + \mathbb{E}_{m \sim q_\psi} \left[\log \frac{q_\psi(m)}{p(m)} \nabla_\psi \log q_\psi(m) \right]. \quad (17)$$

In practice, the variance of this estimator can be very high. However, techniques exist to reduce this variance (30; 34; 28) for general applications. We use a control variate ς in the form

$$\nabla_\psi \mathcal{L}(\psi, \phi) = \mathbb{E}_{m \sim q_\psi} [g(\phi, \psi, \varsigma) \nabla_\psi \log q_\psi(m)], \quad (18)$$

where

$$g(\phi, \psi, \varsigma) = \mathbb{E}_{\mathbf{z} \sim \nu_{d_{\max}}} [\log h_\phi(\mathbf{z} | m) + \log q_\psi(m) - \log p(m) - \varsigma]. \quad (19)$$

We compute ς using the method described in Appendix D.1 (full description in Appendix D).

As mentioned earlier, the benefit of using MCG for variational parameter estimation is the flexibility of choice for q_ψ . In this paper, we compare two choices: (1) MCG of the logits of a standard categorical distribution, and (2) MCG of multi-layer perceptron weights that parameterise a configuration of the MADE neural autoregressive density estimator of Germain et al. (15) (see Appendix F.7). When $|\mathcal{M}|$ is large, such implementations of q_ψ permit an efficient approximate representation of the true model distribution.

3.4 Controlling the optimization

An issue of practical importance is that the convergence of $\psi \rightarrow \psi^*$ is dependent on the convergence of $\phi \rightarrow \phi^*$. Conversely, optimal sample-efficiency for the inference of ϕ is achieved when $\psi \approx \psi^*$. This is intuitive because q_ϕ should “focus” primarily on the highest probability models such that variability in the approximation is minimized efficiently overall. Therefore, it is of some importance to control the variance of the estimates for q_ψ as discussed above. For our implementation, bounding the information gain on the models categorical distribution $q_{\psi_t} \rightarrow q_{\psi_{t+1}}$ provided a practical way to stabilize the optimization process, similar to successful approaches in the reinforcement learning literature (38). We provide further details on our implementation in Appendix D.2.

4 Related work

Conditional normalizing flows (47; 11) have emerged as powerful tools for incorporating conditioning information. Existing methods use the context variable as a conditioning input, but fewer adapt the flow architecture itself. An exception is the transport-based reversible jump MCMC method (7), which learns proposals for transdimensional moves, but does not readily allow its use as an inverse autoregressive flow (22). In contrast, we introduce an identity-parameterized CoSMIC transformation without identity-map training. We bypass path-wise approximations to discrete distributions (19; 27), instead comparing Monte Carlo gradient estimation (28) with Bayesian optimization (39). We adopt an information-based approach to scale gradient steps using “small steps,” inspired by reinforcement learning (38). Bayesian methods for model selection and optimization have advanced with black-box variational inference (34; 45; 46) and flexible flows (36; 31; 11). Recent work in amortized Bayesian mixture models (24) shows amortization over multiple mixture components using conditional normalizing flows, but not for variable dimensions. Conversely, Li et al. (26) introduces an architecture for learning imputation over transdimensional inputs, but lacks immediate application as a variational density. Our approach unifies transdimensional inference with flow-based variational methods, bypassing the need for tailored dimension jumps and broadening applications.

5 Experiments

We present experiments involving synthetic and real data on two representative applications: robust variable selection and directed acyclic graphs. To evaluate the quality of the approximation $q_{\psi, \phi}(m, \theta_m)$ to the target distribution $\pi(m, \theta_m)$ for a relatively small $|\mathcal{M}| < 2^{19}$ model space, we use the *average negative log-likelihood* (NLL) computed over a set of samples drawn from π via a baseline sampling method, in this case reversible jump MCMC (40). Let $\{(m^i, \theta_m^i)\}_{i=1}^N$ denote N independent samples from $\pi(m, \theta_m)$. The average NLL corresponds to the *cross-entropy* $H(\pi, q_{\psi, \phi})$ between the distributions π and $q_{\psi, \phi}$, which quantifies the expected number of bits needed to encode samples from π using the distribution $q_{\psi, \phi}$, and is defined as $\text{NLL} = \frac{1}{N} \sum_{i=1}^N -\log q_{\psi, \phi}(m^i, \theta_m^i)$. Standard metrics Kummerfeld and Rix (25) can compare VTI DAG inference quality with baseline frequentist approaches.

5.1 Bayesian misspecified robust variable selection

We study a robust Bayesian variable selection problem where the response $y \in \mathbb{R}$ is related to predictors $\mathbf{x} \in \mathbb{R}^p$ (including an intercept) through a linear model. The innovation is a mixture-of-Gaussians noise specification, accommodating outliers via a heavy-tailed component. A subset indicator $\gamma \in \{0, 1\}^p$ selects which predictors enter the model. If $\beta \in \mathbb{R}^p$ are the coefficients, only the components where $\gamma_j = 1$ contribute to the linear predictor. In particular, for data $\{(\mathbf{x}_i, y_i)\}_{i=1}^n$ the prediction function is $\mu(\mathbf{x}) = \mathbf{x}^\top(\beta \odot \gamma)$, the likelihood is

$$p(y_i | \mathbf{x}_i, \beta, \gamma) = \mu(\mathbf{x}_i) + (1 - \alpha) \mathcal{N}(y_i; 0, \sigma_1^2) + \alpha \mathcal{N}(y_i; 0, \sigma_2^2), \quad (20)$$

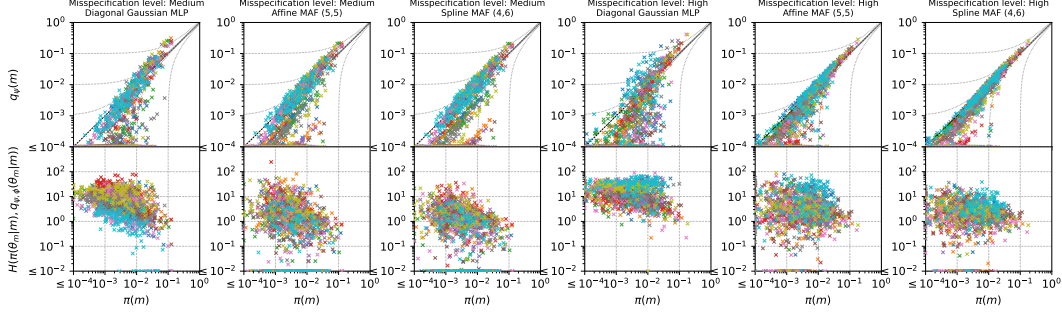


Figure 2: Quality of VTI approximation for Bayesian misspecified robust variable selection. Top row: Estimated model probabilities $q_{\psi, \phi}(m)$ vs true model probabilities $\pi_{\psi, \phi}(m)$ on the log scale. Bottom row: Cross entropy between individual model estimates $q_{\psi, \phi}(\theta_m|m)$ and true density $\pi(\theta_m|m)$ versus true model probability. Colors indicate 10 replicated analyses, each with $|\mathcal{M}| = 2^7 = 128$ models. Columns indicate different normalizing flow constructions for a medium and high misspecified model, increasing flow expressivity from left to right. The flow types are a diagonal Gaussian (Diagonal Gaussian MLP), affine masked autoregressive flow composed of 5 layers each with 5 blocks (Affine MAF (5,5)), and a rational quadratic spline masked autoregressive flow composed of 4 layers each with 6 blocks (Spline MAF (4,6)) (see Appendix A.2 for details).

and priors $p(\gamma) = 2^{-p}$ and $p(\beta) = \mathcal{N}(0, \sigma_\beta^2 \mathbf{I})$. Here, α controls the fraction of outliers, and (σ_1^2, σ_2^2) encode the variances of in-distribution and outliers, respectively. To complicate the inference problem, two misspecified data-generating processes were used, where a medium-misspecified DGP sets $\sigma_1 = 2, \sigma_2 = 5$ and a high-misspecified DGP sets $\sigma_1 = 4, \sigma_2 = 4$. This subverts the unimodality of each $\pi(\theta_m|m)$ such that each becomes a multi-modal distribution that is difficult to sample and also approximate. Table 2 in Appendix E summarizes the full experiment configuration. Figure 2 shows how increasing complexity of the variational density (left-to-right panels) improves the quality of the approximations of both $\pi(\theta_m|m)$ (bottom row) and estimated model probabilities (top row), and that the approximation quality of $\pi(\theta_m|m)$ is higher for higher probability models. Appendix E shows further results for larger $|\mathcal{M}|$, and demonstrates VTI robustness to diffuse priors.

5.2 Bayesian non-linear directed acyclic graph discovery

We consider a dataset of real-valued observations, denoted by $\mathbf{X} \in \mathbb{R}^{n \times N_d}$, where n is the number of data samples and N_d is the number of nodes. Our goal is to perform Bayesian inference over a space of non-linear structural equation models (SEMs) which is isomorphic to a space of directed acyclic graphs (DAGs) and non-linear functions over the active edges. A DAG is represented by a directed adjacency matrix $\mathbf{A} \in \{0, 1\}^{N_d \times N_d}$, where $A_{ij} = 1$ indicates a directed edge from node i to node j and $A_{ij} = 0$ otherwise. The acyclicity constraint requires that the directed edges in \mathbf{A} do not form any directed cycle. In a *non-linear* SEM, each node X_j depends non-linearly on its parents in the form $\mathbf{X} = f(\mathbf{X}) + \epsilon$, $\epsilon_j \sim \mathcal{N}(0, \sigma^2)$, where $f: \mathbb{R}^{N_d} \mapsto \mathbb{R}^{N_d}$ is a nonlinear function possessing an acyclic Jacobian matrix. We follow Bello et al. (1); Thompson et al. (44) whereby f is a multi-layer-perceptron (MLP) structured as $f(\mathbf{X}) = (f_1(\mathbf{X}), \dots, f_{N_d}(\mathbf{X}))^\top$. We implement f using a single hidden layer, with rectified linear unit (ReLU) activation functions used to model non-linearity where the bias term can be optionally included (see Appendix F for details). Acyclicity is enforced by introducing a topological ordering of the N_d nodes. By letting \mathbf{P} be a permutation matrix that reorders nodes into a valid topological order, and defining \mathbf{U} to be strictly upper-triangular, we can represent any acyclic adjacency matrix as $\mathbf{A} = \mathbf{P}^\top \mathbf{U} \mathbf{P}$. Each edge is guaranteed to point from lower-indexed nodes to higher-indexed nodes *in the topological order* (3). Note that this parametrization does not conform to Proposition 3.1, as the correspondence between (\mathbf{P}, \mathbf{U}) and \mathbf{A} is not one-to-one. However, we can circumvent this by sampling with a MADE-based discrete distribution (15) q_ψ for inference over a very high cardinality model space (see Appendices F.8 and F.7 for details). See Appendix F.4 for details of the simulation study in Figure 3, contrasting VTI with the baseline DAGMA (1).

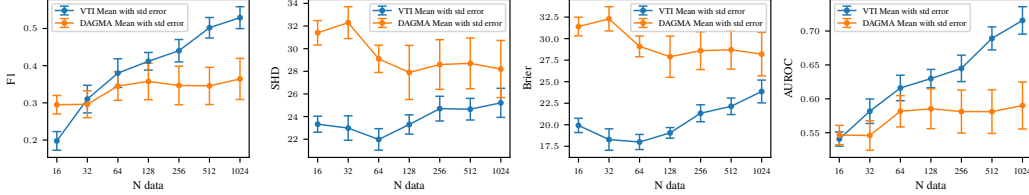


Figure 3: Simulation study comparing VTI to DAGMA (1) for discovery of a 10-node non-linear DAG visualized using standard metrics (Appendix F.2, left to right, where better is: higher, lower, higher). Bars display mean and standard error over 10 i.i.d. repetitions for each data set size.

Real data example in flow cytometry: Sachs et al. (37) utilize Bayesian networks to analyze multi-parameter single-cell data for deriving causal influences in cellular signaling networks of human immune cells. Causal interactions are validated by comparing to a domain-scientist “agreed” adjacency matrix representing causality within the data, establishing a baseline for causal prediction accuracy. We use VTI to discover the distribution of non-linear DAGs for these data, comprising $n = 7466$ entries over $N_d = 11$ nodes, and benchmark this against the agreed adjacency. Table 1 shows the strong performance of VTI posterior approximation compared to state of the art methods.

Method	F1	SHD	Brier	AUROC
VTI Non-linear DAG	0.61	15.0	15.0	0.79
DAGMA Non-linear	0.32	25.0	25.0	0.60

Table 1: Comparison of VTI non-linear DAG formulation for parameters on data from Sachs et al. (37) compared to a baseline DAGMA non-linear (1) approach.

6 Discussion

We have introduced CoSMIC normalizing flows as a means to implement amortized variational transdimensional inference (VTI), the approximation of a target density over a transdimensional space with a single variational density. VTI is broadly applicable to a wide class of transdimensional inference problems, and we have shown its utility in representative problems involving misspecified robust variable selection and non-linear DAG discovery. We have presented two approaches for simultaneously optimizing the variational parameters ψ, ϕ , each with benefits and drawbacks. We have also derived approximation error bounds for our Gaussian surrogate-based approach and established convergence guarantees for the marginal models distribution under convergent optimization steps. The choice of model sampler is dependent on the cardinality of the model space. When $|\mathcal{M}|$ is below the computational memory limit, the Gaussian process surrogate-based sampler is recommended. For high cardinality problems we recommend a neural model sampler for approximate inference on the distribution of model weights using Monte Carlo gradients for SGD optimization.

There are several avenues for future research in CoSMIC flows and VTI. As the variational objective $\mathcal{L}(\psi, \phi)$ (equation 10) returns a single loss value while taking an expectation over $q_\psi(m)$, the VTI approximation quality possesses two notable characteristics. The first is that those models $m \in \mathcal{M}$ estimated to have large posterior model probabilities will contribute most significantly to the loss. Hence the CoSMIC flow will produce a relatively more accurate (in the KL sense) approximation of such models. Conversely those models with low posterior model probability will have relatively worse variational approximations. This effect is seen in Figure 2 (bottom row), regardless of normalizing flow expressivity. While one might prefer greater accuracy on more dominant models, structured changes to $\mathcal{L}(\psi, \phi)$, e.g. weighted stratifications of models across various partitions, could give greater control over where the quality of the variational approximation should focus. The second characteristic is that when the conditional normalising flow is unable to approximate the conditional target $\pi(\theta_m | m)$ well, a smaller loss can be achieved by shrinking the estimated model probability $q_\psi(m)$ to zero. This effect is seen in Figure 2 (top row), which lessens as flow expressivity increases. Here the question is how to design the normalizing flow, i.e. the flow context ξ and the mapping

$C(m)$, to best allocate resources to producing good approximations of those models likely to be of relatively high posterior model probability? E.g., in many transdimensional problems, such as robust misspecified variable selection problem (Section 5.1), models adjacent (e.g. by flipping the state of a single γ_j) to models with high posterior model probability are also high model probability candidates.

Future work can also derive convergence rates, which will depend on the choice of optimization algorithm for the flow parameters. In addition, our analysis for the surrogate-based approach is general enough to be extended to a variety of methods for approximating a models' distribution.

References

- [1] Bello, K., Aragam, B., and Ravikumar, P. (2022). DAGMA: Learning DAGs via M-matrices and a Log-Determinant Acyclicity Characterization. In *Advances in Neural Information Processing Systems*.
- [2] Blei, D. M., Kucukelbir, A., and McAuliffe, J. D. (2017). Variational Inference: A Review for Statisticians. *Journal of the American Statistical Association*, 112(518):859–877.
- [3] Bonilla, E. V., Elinas, P., Zhao, H., Filippone, M., Kitsios, V., and O’Kane, T. (2024). Variational DAG Estimation via State Augmentation With Stochastic Permutations.
- [4] Boucheron, S., Lugosi, G., and Massart, P. (2013). *Concentration Inequalities: A Nonasymptotic Theory of Independence*.
- [5] Brooks, S. P., Giudici, P., and Roberts, G. O. (2003). Efficient Construction of Reversible Jump Markov Chain Monte Carlo Proposal Distributions. *Journal of the Royal Statistical Society Series B: Statistical Methodology*, 65(1):3–39.
- [6] Bubeck, S. and Cesa-Bianchi, N. (2012). *Regret Analysis of Stochastic and Nonstochastic Multi-Armed Bandit Problems*, volume 5. Boston.
- [7] Davies, L., Salomone, R., Sutton, M., and Drovandi, C. (2023). Transport Reversible Jump Proposals. In *Proceedings of The 26th International Conference on Artificial Intelligence and Statistics*, pages 6839–6852.
- [8] Dayan, P., Hinton, G. E., Neal, R. M., and Zemel, R. S. (1995). The Helmholtz Machine. *Neural Computation*, 7(5):889–904.
- [9] Diluvi, G. C., Bloem-Reddy, B., and Campbell, T. (2024). Mixed variational flows for discrete variables. In *Proceedings of The 27th International Conference on Artificial Intelligence and Statistics*, pages 2431–2439.
- [10] Dubins, L. E. and Freedman, D. A. (1965). A Sharper Form of the Borel-Cantelli Lemma and the Strong Law. *The Annals of Mathematical Statistics*, 36(3):800–807.
- [11] Durkan, C., Bekasov, A., Murray, I., and Papamakarios, G. (2019). Neural Spline Flows. In *Advances in Neural Information Processing Systems*, volume 32.
- [12] Durkan, C., Bekasov, A., Murray, I., and Papamakarios, G. (2020). Nflows: Normalizing flows in PyTorch. Zenodo.
- [13] Gabri , M., Rotskoff, G. M., and Vanden-Eijnden, E. (2022). Adaptive Monte Carlo augmented with normalizing flows. *Proceedings of the National Academy of Sciences*, 119(10):e2109420119.
- [14] Gelman, A. and Yao, Y. (2020). Holes in Bayesian statistics*. *Journal of Physics G: Nuclear and Particle Physics*, 48(1):014002.
- [15] Germain, M., Gregor, K., Murray, I., and Larochelle, H. (2015). MADE: Masked Autoencoder for Distribution Estimation. In *Proceedings of the 32nd International Conference on Machine Learning*, pages 881–889.
- [16] Gijsberts, A. and Metta, G. (2013). Real-time model learning using Incremental Sparse Spectrum Gaussian Process Regression. *Neural Networks*, 41:59–69.
- [17] Green, P. J. (1995). Reversible jump Markov chain Monte Carlo computation and Bayesian model determination. *Biometrika*, 82(4):711–732.
- [18] Heckerman, D., Meek, C., and Cooper, G. (2006). A Bayesian Approach to Causal Discovery. In Holmes, D. E. and Jain, L. C., editors, *Innovations in Machine Learning: Theory and Applications*, pages 1–28. Berlin, Heidelberg.

- [19] Jang, E., Gu, S., and Poole, B. (2017). Categorical Reparameterization with Gumbel-Softmax. In *International Conference on Learning Representations*.
- [20] Jordan, M. I., Ghahramani, Z., Jaakkola, T. S., and Saul, L. K. (1999). An Introduction to Variational Methods for Graphical Models. *Machine Learning*, 37(2):183–233.
- [21] Kingma, D. P. and Ba, J. (2017). Adam: A Method for Stochastic Optimization.
- [22] Kingma, D. P., Salimans, T., Jozefowicz, R., Chen, X., Sutskever, I., and Welling, M. (2016). Improved Variational Inference with Inverse Autoregressive Flow. In *Advances in Neural Information Processing Systems*, volume 29.
- [23] Kingma, D. P. and Welling, M. (2013). Auto-Encoding Variational Bayes.
- [24] Kucharsky, S. and Burkner, P. C. (2025). Amortized Bayesian Mixture Models.
- [25] Kummerfeld, E. and Rix, A. (2019). Simulations evaluating resampling methods for causal discovery: Ensemble performance and calibration.
- [26] Li, Y., Akbar, S., and Oliva, J. (2020). ACFlow: Flow Models for Arbitrary Conditional Likelihoods. In *Proceedings of the 37th International Conference on Machine Learning*, pages 5831–5841.
- [27] Maddison, C. J., Mnih, A., and Teh, Y. W. (2017). The Concrete Distribution: A Continuous Relaxation of Discrete Random Variables. In *International Conference on Learning Representations*.
- [28] Mohamed, S., Rosca, M., Figurnov, M., and Mnih, A. (2020). Monte Carlo Gradient Estimation in Machine Learning. *Journal of Machine Learning Research*, 21(132):1–62.
- [29] O’Hara, R. B. and Sillanpää, M. J. (2009). A review of Bayesian variable selection methods: What, how and which. *Bayesian Analysis*, 4(1):85–117.
- [30] Paisley, J., Blei, D. M., and Jordan, M. I. (2012). Variational Bayesian inference with stochastic search. In *Proceedings of the 29th International Conference on Machine Learning*, ICML’12, pages 1363–1370, Madison, WI, USA.
- [31] Papamakarios, G., Pavlakou, T., and Murray, I. (2017). Masked Autoregressive Flow for Density Estimation. In *Advances in Neural Information Processing Systems*, volume 30.
- [32] Papamakarios, G., Sterratt, D., and Murray, I. (2019). Sequential Neural Likelihood: Fast Likelihood-free Inference with Autoregressive Flows. In *Proceedings of the Twenty-Second International Conference on Artificial Intelligence and Statistics*, pages 837–848.
- [33] Pisier, G. (2016). Subgaussian sequences in probability and Fourier analysis. *Graduate Journal of Mathematics*, 1:59–78.
- [34] Ranganath, R., Gerrish, S., and Blei, D. M. (2014). Black Box Variational Inference. In *Proceedings of the 17th International Conference on Artificial Intelligence and Statistics (AISTATS)*, Reykjavik, Iceland.
- [35] Rasmussen, C. E. and Williams, C. K. I. (2006). *Gaussian Processes for Machine Learning*. Cambridge, MA.
- [36] Rezende, D. and Mohamed, S. (2015). Variational Inference with Normalizing Flows. In *Proceedings of the 32nd International Conference on Machine Learning*, pages 1530–1538.
- [37] Sachs, K., Perez, O., Pe’er, D., Lauffenburger, D. A., and Nolan, G. P. (2005). Causal Protein-Signaling Networks Derived from Multiparameter Single-Cell Data. *Science*, 308(5721):523–529.
- [38] Schulman, J., Wolski, F., Dhariwal, P., Radford, A., and Klimov, O. (2017). Proximal Policy Optimization Algorithms.
- [39] Shahriari, B., Swersky, K., Wang, Z., Adams, R. P., and de Freitas, N. (2016). Taking the Human Out of the Loop: A Review of Bayesian Optimization. *Proceedings of the IEEE*, 104(1):148–175.
- [40] Sisson, S. A. (2005). Transdimensional Markov Chains: A Decade of Progress and Future Perspectives. *Journal of the American Statistical Association*, 100(471):1077–1089.
- [41] Srinivas, N., Krause, A., Kakade, S., and Seeger, M. (2010). Gaussian process optimization in the bandit setting: No regret and experimental design. In *Proceedings of the 27th International Conference on Machine Learning*, ICML’10, pages 1015–1022, Madison, WI, USA.

- [42] Srinivas, N., Krause, A., Kakade, S. M., and Seeger, M. (2012). Gaussian Process Optimization in the Bandit Setting: No Regret and Experimental Design. *IEEE Transactions on Information Theory*, 58(5):3250–3265.
- [43] Steinberg, D. M., Oliveira, R., Ong, C. S., and Bonilla, E. V. (2024). Variational Search Distributions. In *NeurIPS 2024 Workshop on Bayesian Decision-making and Uncertainty*.
- [44] Thompson, R., Bonilla, E. V., and Kohn, R. (2025). ProDAG: Projection-Induced Variational Inference for Directed Acyclic Graphs.
- [45] Titsias, M. and Lázaro-Gredilla, M. (2014). Doubly Stochastic Variational Bayes for non-Conjugate Inference. In *Proceedings of the 31st International Conference on Machine Learning*, pages 1971–1979.
- [46] Wingate, D. and Weber, T. (2013). Automated Variational Inference in Probabilistic Programming.
- [47] Winkler, C., Worrall, D., Hoogetboom, E., and Welling, M. (2019). Learning Likelihoods with Conditional Normalizing Flows.
- [48] Zammit-Mangion, A., Sainsbury-Dale, M., and Huser, R. (2024). Neural Methods for Amortized Inference. *Annual Review of Statistics and Its Application*.

A Construction and analysis of a CoSMIC normalizing flow

CoSMIC IAF procedure: Draw reference samples

$$\mathbf{z} = (z^{(1)}, \dots, z^{(d_{\max})}) \sim \nu_{d_{\max}}.$$

For a given m , define the permutation matrix P_m that groups active coordinates first:

$$(\mathbf{z}_m, \mathbf{z}_{\setminus m}) := P_m \mathbf{z} \implies \mathbf{z}_m \in \mathbb{R}^{d_m}, \mathbf{z}_{\setminus m} \in \mathbb{R}^{\setminus d_m}, \setminus d_m = d_{\max} - d_m.$$

Concatenate the coordinate-wise transforms τ_{ρ_i} into the map T_ϕ and bookend with permutations P_m to give the strict CoSMIC bijection

$$T_\phi^{(P_m)}(\mathbf{z}) := P_m^{-1}(\tau_{\rho_1^{C(m)}}(\mathbf{z}^{(1)}), \dots, \tau_{\rho_{d_{\max}}^{C(m)}}(\mathbf{z}^{(d_{\max})})) P_m.$$

Proof of Proposition 2.2. (a)–(b) Density factorization and marginal consistency.

We aim to prove

$$\begin{aligned} \text{(a)} \quad & \tilde{q}_\phi^{(P_m)}(\boldsymbol{\theta}_m, \mathbf{u}_{\setminus m} \mid m) = q_\phi(\boldsymbol{\theta}_m \mid m) \nu_{d_{\setminus m}}(\mathbf{u}_{\setminus m}), \\ \text{and so (b)} \quad & \int \tilde{q}_\phi^{(P_m)}(\boldsymbol{\theta}_m, \mathbf{u}_{\setminus m} \mid m) d\mathbf{u}_{\setminus m} = q_\phi(\boldsymbol{\theta}_m \mid m). \end{aligned}$$

Write $T_\phi^{(P_m), -1} = (T_{\phi, m}^{-1}, \text{Id})$, where Id denotes the identity transform, and let the permuted reference vector be $P_m \mathbf{z} = (\mathbf{z}_m, \mathbf{z}_{\setminus m}) \in \mathbb{R}^{d_m} \times \mathbb{R}^{d_{\setminus m}}$. Because the masking function C sets every transform τ_{ρ_i} with $C_i(m) = 0$ to the identity, the inverse flow splits as

$$T_\phi^{(P_m), -1}(\boldsymbol{\theta}_m, \mathbf{u}_{\setminus m}) = (T_{\phi, m}^{-1}(\boldsymbol{\theta}_m), \mathbf{u}_{\setminus m}),$$

where $T_{\phi, m}^{-1} : \Theta_m \rightarrow \mathbb{R}^{d_m}$ is the active block and the dummy block is exactly the identity. Consequently, the Jacobian matrix of $T_\phi^{(P_m), -1}$ is block upper-triangular with $\det \nabla T_\phi^{(P_m), -1} = \det \nabla T_{\phi, m}^{-1} \times 1$.

Apply change-of-variables with $\nu_{d_{\max}} = \nu_{d_m} \otimes \nu_{d_{\setminus m}}$ to obtain

$$\begin{aligned} \tilde{q}_\phi^{(P_m)}(\boldsymbol{\theta}_m, \mathbf{u}_{\setminus m} \mid m) &= \nu_{d_{\max}}(T_\phi^{(P_m), -1}(\boldsymbol{\theta}_m, \mathbf{u}_{\setminus m})) |\det \nabla T_\phi^{(P_m), -1}| \\ &= \nu_{d_m}(T_{\phi, m}^{-1}(\boldsymbol{\theta}_m)) \nu_{d_{\setminus m}}(\mathbf{u}_{\setminus m}) |\det \nabla T_{\phi, m}^{-1}(\boldsymbol{\theta}_m)| \\ &= q_\phi(\boldsymbol{\theta}_m \mid m) \nu_{d_{\setminus m}}(\mathbf{u}_{\setminus m}), \end{aligned}$$

which proves the factorization (a).

Integrating the right-hand side over $\mathbf{u}_{\setminus m}$ recovers (b) $q_\phi(\boldsymbol{\theta}_m \mid m)$, completing the proof. \square

Proof of Corollary 2.3. It is sufficient to show $D_{\text{KL}}(\tilde{q}_{\psi, \phi} \parallel \tilde{\eta}) = D_{\text{KL}}(q_{\psi, \phi} \parallel \eta) := \mathcal{L}(\psi, \phi)$. Note by equation 3, $\tilde{\eta}(m, \boldsymbol{\theta}_m, \mathbf{u}_{\setminus m}) = p(m) \tilde{\eta}(\boldsymbol{\theta}_m, \mathbf{u}_{\setminus m} \mid m) = p(m) \eta(\boldsymbol{\theta}_m \mid m) \nu_{d_{\setminus m}}(\mathbf{u}_{\setminus m})$.

$$\begin{aligned} D_{\text{KL}}(\tilde{q}_{\psi, \phi} \parallel \tilde{\pi}) &= \mathbb{E}_{m \sim q_\psi} \left[\mathbb{E}_{(\boldsymbol{\theta}_m, \mathbf{u}_{\setminus m}) \sim \tilde{q}_\phi} \left[\log \left(\frac{q_\psi(m) \tilde{q}_\phi(\boldsymbol{\theta}_m, \mathbf{u}_{\setminus m} \mid m)}{p(m) \tilde{\eta}(\boldsymbol{\theta}_m, \mathbf{u}_{\setminus m} \mid m)} \right) \right] \right] \\ &= \mathbb{E}_{m \sim q_\psi} \left[\mathbb{E}_{(\boldsymbol{\theta}_m, \mathbf{u}_{\setminus m}) \sim \tilde{q}_\phi} \left[\log \left(\frac{\tilde{q}_\phi(\boldsymbol{\theta}_m, \mathbf{u}_{\setminus m} \mid m)}{\tilde{\eta}(\boldsymbol{\theta}_m, \mathbf{u}_{\setminus m} \mid m)} \right) \right] + \log(q_\psi(m)) - \log(p(m)) \right] \\ &= \mathbb{E}_{m \sim q_\psi} [\log(q_\psi(m)) - \log(p(m))] + \\ &\quad \mathbb{E}_{m \sim q_\psi} \left[\mathbb{E}_{\mathbf{z} \sim \nu_{d_{\max}}} \left[\log \left(\frac{\nu_{d_m}(\mathbf{z}_{d_m}) \nu_{d_{\setminus m}}(\mathbf{z}_{\setminus m}) |\det \nabla T_\phi(\mathbf{z})|^{-1}}{\eta(\boldsymbol{\theta}_m \mid m) \nu_{d_{\setminus m}}(\mathbf{u}_{\setminus m})} \right) \right] \right] \quad \text{by Proposition 2.2} \\ &= D_{\text{KL}}(q_{\psi, \phi} \parallel \pi) \\ &= \mathcal{L}(\psi, \phi). \end{aligned}$$

\square

A.1 CoSMIC IAF computational complexity

Corollary A.1 (Computational complexity).

- Sampling (forward IAF): *all coordinates can be updated in parallel* $\Rightarrow \mathcal{O}(1)$ wall-time depth.
- Evaluation (inverse direction): *must populate $\mathbf{z}^{(<i)}$ sequentially* $\Rightarrow \mathcal{O}(d_{\max})$ arithmetic operations, identical to a standard IAF.

Proof. The forward IAF updates θ_m via closed-form τ_i that read *previous outputs*—all available after one pass through the network—which are thereby fully parallelizable. Conversely, evaluating $T_\phi^{(m),-1}$ at an arbitrary point in $\Theta_m \times \mathcal{M}$ must reconstruct \mathbf{z} sequentially, exactly as for any IAF, giving $\mathcal{O}(d_{\max})$ time. \square

A.2 Experimental CoSMIC transform compositions

The experiments use the below compositions of transforms as inverse autoregressive flows $T_\phi(\mathbf{z} \mid m)$ where \mathbf{z} are the inputs from the reference distribution and m is the context input. All compositions except for the diagonal Gaussian are assumed to have the strict left-right permutations discussed in Appendix A. The term “block” is defined in Appendix A.3.

Context encoder: Experiments will sometimes use a context encoder that projects the context input to a higher dimensional space. Typically this will take the form of a multi-layered perceptron with hidden layers of increasing size (fixed to powers of 2) and terminating in an activation layer at the largest size, say 2^{12} nodes.

Model-specific reverse-permutation: Flow compositions commonly include reverse permutations to ensure expressibility of an autoregressive-NN-based flow is (approximately) the same for all coordinates. Denoting the generic reverse permutation for all coordinates as P^{rev} , we assume the strict left-right permutation P_m (as per Appendix A) has been applied, and hence define the left-most d_m -coordinate reverse permutation $P_{<d_m}^{\text{rev}}$.

Affine(5,5): The learned component is the affine masked autoregressive transform (31), denoted here as $T_{\phi_k}^{\text{Affine}}$ for transforms $k = 1, \dots, 5$, each having 5 blocks. We set $T_\phi := T_{\phi_5}^{\text{Affine}} \circ P_{<d_m}^{\text{rev}} \circ \dots \circ P_{<d_m}^{\text{rev}} \circ T_{\phi_1}^{\text{Affine}}$.

Spline(4,6): The learned component is the rational quadratic spline masked autoregressive flow architecture (11), denoted here as $T_{\phi_k}^{\text{RQ-Spline}}$. Each $T_{\phi_k}^{\text{RQ-Spline}}$ has 6 blocks. Additionally, we define a fixed global affine transform T_{μ_g, σ_g} that is not dependent on inputs nor context and hence has only two learnable parameters: scale μ_g and shift σ_g . We set $T_\phi := T_{\mu_g, \sigma_g} \circ T_{\phi_5}^{\text{RQ-Spline}} \circ P_{<d_m}^{\text{rev}} \circ \dots \circ P_{<d_m}^{\text{rev}} \circ T_{\phi_1}^{\text{RQ-Spline}}$.

A.3 Autoregressive flow definitions

We use the residual variant of the Masked Autoencoder for Distribution Estimation (MADE) (15), implemented in PyTorch by (12). Each block maintains the autoregressive property by assigning degrees $\{1, \dots, d\}$ to inputs and propagating them forward.

Given input $\mathbf{x} \in \mathbb{R}^d$ and optional context \mathbf{z} , each residual block computes:

$$\mathbf{h} = \mathbf{x} + \text{MaskedLinear}_2(\sigma(\text{BN}_2(\text{MaskedLinear}_1(\sigma(\text{BN}_1(\mathbf{x}))) + \delta(\mathbf{z}))))).$$

Here, MaskedLinear_i are masked linear layers respecting the autoregressive structure, BN_i are optional batch norm layers, and $\delta(\mathbf{z})$ is an optional context projection. All layers preserve feature dimensionality and respect degree ordering to ensure autoregressive validity.

B Theoretical analysis of the model weights distribution

We consider the following bi-level stochastic optimization problem over a function $f : \mathcal{M} \times \Phi \rightarrow \mathbb{R}$ as:

$$\phi^* \in \arg \max_{\phi \in \Phi} \max_{q_f \in \mathcal{P}(\mathcal{M})} \mathbb{E}_{m \sim q} [f(m, \phi) + \log p(m)] + H[q_f] = \arg \max_{\phi \in \Phi} \mathbb{E}_{m \sim q_{f, \phi}^*} [f(m, \phi) + \log p(m)], \quad (21)$$

where $\mathcal{P}(\mathcal{M})$ denotes the space of probability measures over \mathcal{M} , H is the entropy, and the optimal q_f for a given ϕ can be shown to be:

$$q_{f, \phi}^*(m) := \frac{p(m) \exp f(m, \phi)}{\sum_{m' \in \mathcal{M}} p(m') \exp f(m', \phi)}, \quad m \in \mathcal{M}. \quad (22)$$

This formulation corresponds to a stochastic optimization problem over two variables ϕ and q_f , where the optimum for q_f has a closed-form expression $q_{f, \phi}^*$ for every given $\phi \in \Phi$. To solve this problem, we will follow a sequential optimization process over ϕ (e.g., stochastic gradient descent). However, sampling from the optimal model distribution $q_{f, \phi}^*$ (above) requires evaluating the summation in the normalization constant, which is expensive. Therefore, we will instead approximate each q_{f, ϕ_t}^* with a distribution $q_{u, t}$ composed of a cheaper-to-evaluate surrogate u_t based on noisy observations $y_{t-1, i} = \tilde{f}(\mathbf{z}_i, m_i, \phi_{t-1})$, where $\mathbf{z}_i \sim \nu$ and $m_i \sim q_{u, t-1}$, $i \in \{1, \dots, B\}$, such that $\mathbb{E}_{\mathbf{z} \sim \nu} [\tilde{f}(\mathbf{z}, m, \phi)] = f(m, \phi)$. If we ensure that $q_{u, t}$ approaches q_{f, ϕ_t}^* over time, optimization steps based on $q_{u, t}$ will eventually follow q_{f, ϕ_t}^* and allow for the optimum ϕ^* to be reached.

B.1 Regularity assumptions

We make the following assumptions about the function f and the observation noise.

Assumption B.1. The objective f is a sample from a zero-mean Gaussian process prior with a bounded, positive-semidefinite covariance function $\kappa : (\mathcal{M} \times \Phi)^2 \rightarrow \mathbb{R}$, which is continuous over Φ .

The GP assumption allows us to derive closed-form expressions for predictions over f and their associated uncertainty. The continuity assumption on κ is easily satisfied by most practical covariance functions and ensures that, if ϕ_t converges to some ϕ^* , GP-based estimates $f(m, \phi^*)$ will also converge for every $m \in \mathcal{M}$. To model predictions over f with closed-form GP updates, we also need Gaussian assumptions about the observation noise, which is given by:

$$\epsilon_{m, \phi} := \tilde{f}(\mathbf{z}, m, \phi) - f(m, \phi), \quad \mathbf{z} \sim \nu, \quad m \in \mathcal{M}, \phi \in \Phi. \quad (23)$$

However, as we will show in our analysis, sub-Gaussian tails are enough for GP modeling, which we formalize next.

Assumption B.2. The observation noise is σ_ϵ^2 -sub-Gaussian, i.e., given any $m \in \mathcal{M}$ and $\phi \in \Phi$, we have:

$$\forall s \in \mathbb{R}, \quad \mathbb{E}[\exp(s\epsilon_{m, \phi})] \leq \exp\left(\frac{1}{2}s^2\sigma_\epsilon^2\right). \quad (24)$$

This mild assumption is satisfied, for example, when ν is a zero-mean Gaussian distribution and \tilde{f} is Lipschitz continuous on its first argument, in which case σ_ϵ only depends on \tilde{f} through its Lipschitz constant (4; 33).

B.2 Gaussian process model

Under the GP assumption $f \sim \mathcal{GP}(0, \kappa)$, the posterior over f is again a Gaussian process. Suppose at each iteration $t \geq 1$ of stochastic gradient descent we sample a mini-batch $\{m_{t, i}\}_{i=1}^B$ from a variational posterior approximating $q_{f, \phi}^*$ at $\phi = \phi_{t-1}$. Given a batch of observations $\mathcal{B}_t := \{\phi_{t-1}, m_{t, i}, y_{t, i}\}_{i=1}^B$, the GP posterior $f|\mathcal{B}_{1, \dots, t} \sim \mathcal{GP}(\mu_t, \kappa_t)$ has its mean and covariance described by the following recursive equations:

$$\mu_t(m, \phi) = \mu_{t-1}(m, \phi) + \kappa_{t-1}(m, \phi)^\top (\mathbf{K}_{t-1} + \sigma_\epsilon^2 \mathbf{I})^{-1} (\mathbf{y}_t - \mu_{t-1}) \quad (25)$$

$$\kappa_t(m, \phi, m', \phi') = \kappa_{t-1}(m, \phi, m', \phi') - \kappa_{t-1}(m, \phi)^\top (\mathbf{K}_{t-1} + \sigma_\epsilon^2 \mathbf{I})^{-1} \kappa_{t-1}(m', \phi), \quad (26)$$

where $\kappa_{t-1}(m, \phi) := [\kappa_{t-1}(m, \phi, m_{t, i}, \phi_{t-1})]_{i=1}^B \in \mathbb{R}^B$, $\mathbf{K}_{t-1} := [\kappa_{t-1}(m_{t, i}, \phi_{t-1}, m_{t, j}, \phi_{t-1})]_{i, j=1}^B \in \mathbb{R}^{B \times B}$, and $\mu_{t-1} := [\mu_{t-1}(m_{t, i}, \phi_{t-1})]_{i=1}^B \in \mathbb{R}^B$, with $\mu_0 = 0$ and $\kappa_0 = \kappa$. Any pointwise prediction is then modeled as $f(m, \phi)|\mathcal{B}_{1, \dots, t} \sim \mathcal{N}(\mu_t(m, \phi), \sigma_t^2(m, \phi))$, where $\sigma_t^2(m, \phi) := \kappa_t(m, \phi, m, \phi)$, for $(m, \phi) \in \mathcal{M} \times \Phi$.

Algorithm 1 Stochastic optimization with UCB sampling

```

for  $t \in \{1, \dots, N\}$  do
   $\{m_{t,i}\}_{i=1}^B \sim q_{u,t-1}$ 
   $\{z_{t,i}\}_{i=1}^B \sim \nu$ 
   $y_{t,i} = f(z_{t,i}, m_{t,i}, \phi_{t-1})$ , for  $i \in \{1, \dots, B\}$ 
   $\phi_t \leftarrow \text{UPDATEPARAMETERS}(\phi_{t-1}, \{\tilde{f}(z_{t,i}, m_{t,i}, \phi_{t-1})\}_{i=1}^B, q_{u,t-1})$ 
   $\mu_t, \kappa_t \leftarrow \text{UPDATESURROGATE}(\{m_{t,i}, y_{t,i}\}_{i=1}^B, \phi_{t-1}, \mu_{t-1}, \kappa_{t-1})$ 
end for

```

B.3 Upper confidence bound (UCB) algorithm

Given the GP posterior, we formulate an upper confidence bound algorithm (41) with:

$$u_t(m) := \mu_t(m, \phi_t) + \beta_t \sigma_t(m, \phi_t), \quad m \in \mathcal{M}, \quad (27)$$

where $\beta_t > 0$ is a parameter controlling the size of the confidence bound, which we will discuss in our analysis. We then derive a sampling distribution based on using the UCB as a surrogate for f as:

$$q_{u,t} \in \arg \max_{q \in \mathcal{P}(\mathcal{M})} \mathbb{E}_{m \sim q} [u_t(m) + \log p(m) - \log q(m)]. \quad (28)$$

The solution to this optimization is available in closed form as the UCB softmax:

$$q_{u,t}(m) = \frac{p(m) \exp u_t(m)}{\sum_{m' \in \mathcal{M}} p(m') \exp u_t(m')}, \quad m \in \mathcal{M}. \quad (29)$$

Equipped with this UCB-based sampling distribution, we follow the generic procedure outlined in Algorithm 1. The algorithm starts by sampling from the current UCB distribution. A sample-based estimate of the optimization objective $\mathbb{E}_{m \sim \phi_t} [f(m, \phi_{t-1})] \approx \frac{1}{B} \sum_{i=1}^B \tilde{f}(z_{t,i}, m_{t,i}, \phi_{t-1})$ is then passed to the algorithm responsible for updating the parameters ϕ_t , e.g., a stochastic gradient descent update. Once the parameters are updated, we reevaluate the objective and update our GP. The procedure then repeats up to a given number of iterations $N \in \mathbb{N}$.

B.4 Approximation errors under sub-Gaussian noise

In the following, we derive generic concentration bounds for GP predictions under sub-Gaussian observation noise. We start by showing that the approximation error between the GP mean and the true function is sub-Gaussian.

Lemma B.1. *Let $f \sim \mathcal{GP}(0, \kappa)$ be a zero-mean Gaussian process with a given positive-definite covariance function $\kappa : \mathcal{S} \times \mathcal{S} \rightarrow \mathbb{R}$. Assume we are given a sequence of observations $y_n = f(x_n) + \epsilon_n$, where $x_n \in \mathcal{S}$ and ϵ_n is σ_ϵ^2 -sub-Gaussian noise, for all $n \in \mathbb{N}$. Let μ_n and σ_n^2 denote the predictive mean and variance, respectively, of the GP posterior under the assumption that the noise is zero-mean Gaussian with variance given by σ_ϵ^2 . Then, for all $n \geq 0$ and all $x \in \mathcal{S}$, we have that $f(x) - \mu_n(x)$ is $\sigma_n^2(x)$ -sub-Gaussian.*

Proof. For $n = 0$, the proof is trivial as, without observations, we only have the prior with $\mu_0(x) = 0$ and $\sigma_0^2(x) = \kappa(x, x)$. Now let $\mathcal{X}_n := \{x_i\}_{i=1}^n \subset \mathcal{S}$ denote a set of $n \geq 1$ observed locations. For any given $x \in \mathcal{S}$, expanding the GP posterior mean from its definition, the approximation error can be decomposed as:

$$\begin{aligned} \Delta_n(x) &:= f(x) - \mu_n(x) = f(x) - \kappa(x, \mathcal{X}_n)(\mathbf{K}_n + \sigma_\epsilon^2 \mathbf{I})^{-1}(\mathbf{f}_n + \boldsymbol{\epsilon}_n) \\ &= f(x) - \kappa(x, \mathcal{X}_n)(\mathbf{K}_n + \sigma_\epsilon^2 \mathbf{I})^{-1} \mathbf{f}_n - \kappa(x, \mathcal{X}_n)(\mathbf{K}_n + \sigma_\epsilon^2 \mathbf{I})^{-1} \boldsymbol{\epsilon}_n, \end{aligned} \quad (30)$$

where $\kappa(x, \mathcal{X}_n) := [\kappa(x, x_1), \dots, \kappa(x, x_n)]$, $\mathbf{K}_n := [\kappa(x_i, x_j)]_{i,j=1}^n$, $\mathbf{f}_n := [f(x_i)]_{i=1}^n$, and $\boldsymbol{\epsilon}_n := [\epsilon_i]_{i=1}^n$. The last term on the right-hand side above is sub-Gaussian, since $\mathbb{E}[\boldsymbol{\epsilon}_n] = 0$ and, letting $\boldsymbol{\alpha}_n := (\mathbf{K}_n + \sigma_\epsilon^2 \mathbf{I})^{-1} \kappa(\mathcal{X}_n, x)$, we have a sum of independent sub-Gaussian random variables, see e.g. (33), Lemma 1.1:

$$\mathbb{E}[\exp(\boldsymbol{\alpha}_n^\top \boldsymbol{\epsilon}_n)] = \mathbb{E} \left[\exp \left(\sum_{i=1}^n \alpha_{n,i} \epsilon_{n,i} \right) \right] = \prod_{i=1}^n \mathbb{E}[\exp(\alpha_{n,i} \epsilon_{n,i})] \leq \exp \left(\frac{1}{2} \sigma_\epsilon^2 \sum_{i=1}^n \alpha_{n,i}^2 \right), \quad (31)$$

which follows from the definition of sub-Gaussian noise (cf. Assumption B.2). The remaining term on the right-hand side of equation 30 is a zero-mean Gaussian random variable with variance given by:

$$\begin{aligned} & \text{Var}[f(x) - \kappa(x, \mathcal{X}_n)(\mathbf{K}_n + \sigma_\epsilon^2 \mathbf{I})^{-1} \mathbf{f}_n] \\ &= \kappa(x, x) - 2\kappa(x, \mathcal{X}_n)(\mathbf{K}_n + \sigma_\epsilon^2 \mathbf{I})^{-1} \kappa(\mathcal{X}_n, x) + \kappa(x, \mathcal{X}_n)(\mathbf{K}_n + \sigma_\epsilon^2 \mathbf{I})^{-1} \mathbf{K}_n (\mathbf{K}_n + \sigma_\epsilon^2 \mathbf{I})^{-1} \kappa(\mathcal{X}_n, x) \\ &= \kappa(x, x) - 2\kappa(x, \mathcal{X}_n)(\mathbf{K}_n + \sigma_\epsilon^2 \mathbf{I})^{-1} \kappa(\mathcal{X}_n, x) + \boldsymbol{\alpha}_n^\top \mathbf{K}_n \boldsymbol{\alpha}_n. \end{aligned} \quad (32)$$

As equation 30 describes the sum of two independent sub-Gaussian random variables, we can follow similar reasoning to the one applied in equation 31 to show that $\Delta_n(x)$ is $s_n^2(x)$ -sub-Gaussian for some $s_n^2(x) > 0$. The resulting sub-Gaussian parameter $s_n^2(x)$ is then bounded by the sum of the individual sub-Gaussian parameters in equations 31 and 32 as:

$$\begin{aligned} s_n^2(x) &\leq \kappa(x, x) - 2\kappa(x, \mathcal{X}_n)(\mathbf{K}_n + \sigma_\epsilon^2 \mathbf{I})^{-1} \kappa(\mathcal{X}_n, x) + \boldsymbol{\alpha}_n^\top \mathbf{K}_n \boldsymbol{\alpha}_n + \sigma_\epsilon^2 \boldsymbol{\alpha}_n^\top \boldsymbol{\alpha}_n \\ &= \kappa(x, x) - 2\kappa(x, \mathcal{X}_n)(\mathbf{K}_n + \sigma_\epsilon^2 \mathbf{I})^{-1} \kappa(\mathcal{X}_n, x) + \boldsymbol{\alpha}_n^\top (\mathbf{K}_n + \sigma_\epsilon^2 \mathbf{I}) \boldsymbol{\alpha}_n \\ &= \kappa(x, x) - 2\kappa(x, \mathcal{X}_n)(\mathbf{K}_n + \sigma_\epsilon^2 \mathbf{I})^{-1} \kappa(\mathcal{X}_n, x) + \kappa(x, \mathcal{X}_n)(\mathbf{K}_n + \sigma_\epsilon^2 \mathbf{I})^{-1} \kappa(\mathcal{X}_n, x) \quad (33) \\ &= \kappa(x, x) - \kappa(x, \mathcal{X}_n)(\mathbf{K}_n + \sigma_\epsilon^2 \mathbf{I})^{-1} \kappa(\mathcal{X}_n, x) \\ &= \sigma_n^2(x), \end{aligned}$$

which concludes the proof. \square

B.5 Convergence guarantees

Now we apply the error bounds above to the general optimization problem in equation 21.

Assumption B.3. The sequence of parameters $\{\phi_t\}_{t=1}^\infty$ is a Cauchy sequence, i.e.:

$$\forall \lambda > 0, \quad \exists N_\lambda \in \mathbb{N} : \quad \|\phi_{t+1} - \phi_t\| \leq \lambda, \quad \forall t \geq N_\lambda. \quad (34)$$

The assumption above can be guaranteed by, e.g., diminishing step sizes during (stochastic) gradient descent. It essentially means that ϕ_t will converge to some $\hat{\phi} \in \Phi \subseteq \mathbb{R}^{n_\phi}$, though not requiring it to be the optimum.

Assumption B.4. The prior $p(m)$ has full support over \mathcal{M} .

Such assumption ensures that the prior would not wrongly assign zero probability to plausible models.

Lemma B.2. Let assumptions B.1 to B.4 hold, and set $\beta_t = \beta > 0$, for all $t \in \{0, 1, 2, \dots\}$. Then the following almost surely holds:

$$\sigma_t^2(m, \phi_t) \in \mathcal{O}(t^{-1}), \quad \forall m \in \mathcal{M}. \quad (35)$$

Proof. Consider the following upper bound on the predictive variance of a GP model (43, Lem. D.3):

$$\forall t \in \mathbb{N}, \quad \sigma_t^2(m, \phi) \leq \frac{\sigma_\epsilon^2 \sigma_0^2(m, \phi)}{\sigma_\epsilon^2 + \sigma_0^2(m, \phi) N_t(m, \phi)}, \quad \forall (m, \phi) \in \mathcal{M} \times \Phi, \quad (36)$$

where $N_t(m, \phi)$ denotes the number of observations collected at $(m, \phi) \in \mathcal{M} \times \Phi$ up to time $t \geq 1$. In addition, letting \mathfrak{H}_t denote the σ -algebra generated by the history of all random variables measurable at time t , and setting $\hat{\phi} := \lim_{t \rightarrow \infty} \phi_t$, the second Borel-Cantelli lemma (10) tells us that:³

$$\forall m \in \mathcal{M}, \quad \lim_{t \rightarrow \infty} N_t(m, \hat{\phi}) = \lim_{t \rightarrow \infty} \sum_{i=1}^t \mathbb{P}[m_t = m \mid \mathfrak{H}_{t-1}]. \quad (37)$$

Therefore, for $\sigma_t^2(m, \hat{\phi}) \rightarrow 0$, we need the series above to diverge. To ensure the latter, we can show that the conditional probabilities in Equation (39) have a nonzero lower bound or, if they converge to zero, that they do so slowly enough.

We now derive a lower bound on the sampling probabilities. First, observe that:

$$\forall t \in \mathbb{N}, \quad \mathbb{E}[\|\mu_t(\cdot, \phi_t)\|_\infty] = \mathbb{E}[\|\mathbb{E}[f(\cdot, \phi_t) \mid \mathfrak{H}_t]\|_\infty] \leq \mathbb{E}[\|f(\cdot, \phi)\|_\infty \mid \mathfrak{H}_t], \quad \forall \phi \in \Phi, \quad (38)$$

³More precisely, the second Borell-Cantelli lemma tells us the two sides are proportional to each other, while equality holds if the right-hand side diverges.

where $\|f(\cdot, \phi)\|_\infty = \sup_{m \in \mathcal{M}} |f(m, \phi)|$ denotes the supremum norm of $f(\cdot, \phi)$, and we applied Jensen's inequality in the last step. Since the kernel κ is continuous and bounded, the sub-Gaussian parameter $\sigma_t^2(\cdot, \phi_t)$ has a maximum in \mathcal{M} , which is finite. As the expected value of the maximum of a finite collection of sub-Gaussian random variables is bounded (see, e.g., 4, Thr. 2.5), it follows that the GP mean μ_t is almost surely bounded at all times (by, e.g., Markov's inequality). Considering the model sampling probabilities and that $p_{\min} := \min_{m \in \mathcal{M}} p(m) > 0$ by Assumption B.4, we then have that the following almost surely holds:

$$\begin{aligned} \forall t \geq 0, \quad \mathbb{P}[m_{t+1} = m \mid \mathfrak{H}_t] &= q_{u,t}(m) \geq \frac{p_{\min} \exp(-\|\mu_t(\cdot, \phi_t)\|_\infty + \beta \sigma_t(m, \phi_t))}{\sum_{m' \in \mathcal{M}} \exp(\|\mu_t(\cdot, \phi_t)\|_\infty + \beta \sigma_t(m', \phi_t))} \\ &\geq \frac{p_{\min} \exp(-2\|\mu_t(\cdot, \phi_t)\|_\infty + \beta \sigma_t(m, \phi_t))}{|\mathcal{M}| \max_{m' \in \mathcal{M}} \exp(\beta \sigma_t(m', \phi_t))}. \end{aligned} \quad (39)$$

As, for every $m \in \mathcal{M}$, the sequence $\{\sigma_t^2(m, \phi_t)\}_{t=0}^\infty$ is non-negative and non-increasing, it has a limit by the monotone convergence theorem. Let $\sigma_* := \lim_{t \rightarrow \infty} \max_{m \in \mathcal{M}} \sigma_t(m, \phi_t)$, and let $m_* \in \mathcal{M}$ be one of the maximizers of $\lim_{t \rightarrow \infty} \sigma_t(\cdot, \phi_t)$. If $\sigma_* > 0$, by Equation 39, we have for m_* that:

$$\begin{aligned} \lim_{t \rightarrow \infty} \mathbb{P}[m_{t+1} = m_* \mid \mathfrak{H}_t] &\geq \lim_{t \rightarrow \infty} \frac{p_{\min} \exp(-2\|\mu_t(\cdot, \phi_t)\|_\infty + \beta \sigma_t(m_*, \phi_t))}{|\mathcal{M}| \max_{m \in \mathcal{M}} \exp(\beta \sigma_t(m, \phi_t))} \\ &= \lim_{t \rightarrow \infty} \frac{p_{\min} \exp(-2\|\mu_t(\cdot, \phi_t)\|_\infty + \beta \sigma_*)}{|\mathcal{M}| \exp(\beta \sigma_*)} \\ &= \lim_{t \rightarrow \infty} \frac{p_{\min} \exp(-2\|\mu_t(\cdot, \phi_t)\|_\infty)}{|\mathcal{M}|} \\ &\geq \frac{p_{\min} \exp(-2\mathbb{E}[\|f(\cdot, \hat{\phi})\|_\infty \mid \mathfrak{H}_\infty])}{|\mathcal{M}|} \\ &=: b_m > 0, \end{aligned} \quad (40)$$

which implies $N_t(m_*, \hat{\phi}) \rightarrow \infty$ by Equation 37. However, in that case, we must have $\sigma_*^2 = \lim_{t \rightarrow \infty} \sigma_t^2(m_*, \phi_t) = 0$ by Equation 36, which is a contradiction. Therefore, $\sigma_* = 0$, and consequently $\lim_{t \rightarrow \infty} \sigma_t(m, \phi_t) \leq \sigma_* = 0$, for all $m \in \mathcal{M}$.

Finally, we show that $\sigma_t^2(\cdot, \phi_t) \in \mathcal{O}(t^{-1})$. As we have seen that $\lim_{t \rightarrow \infty} \sigma_t(\cdot, \phi_t) = 0$ above, applying the limit to equation 39, we see that $\mathbb{P}[m_t = m \mid \mathfrak{H}_{t-1}] \rightarrow b_m > 0$, for each $m \in \mathcal{M}$. Hence, $N_t(m, \phi_t)^{-1} \in \mathcal{O}(t^{-1})$, implying that $\sigma_t^2(\cdot, \phi_t)$ is $\mathcal{O}(t^{-1})$ asymptotically by Equation 37, which concludes the proof. \square

Theorem B.3. *Under the assumptions in Lemma B.2, we have that the following holds in probability:*

$$D_{\text{KL}}(q_{u,t} \| q_{f,\phi_t}^*) \in \mathcal{O}_{\mathbb{P}}(t^{-1/2}), \quad (41)$$

where for a stochastic process $\{\xi_t\}_{t \in \mathbb{N}}$, denoting $\xi_t \in \mathcal{O}_{\mathbb{P}}(g(t))$, for a positive function $g : \mathbb{N} \rightarrow (0, \infty)$, means that:

$$\forall \varepsilon > 0, \quad \exists C_\varepsilon \in (0, \infty), N_\varepsilon \in \mathbb{N} : \quad \mathbb{P}\left[\frac{|\xi_t|}{g(t)} > C_\varepsilon\right] \leq \varepsilon, \quad \forall t \geq N_\varepsilon, \quad (42)$$

or equivalently that:

$$\lim_{C \rightarrow \infty} \limsup_{t \rightarrow \infty} \mathbb{P}\left[\frac{|\xi_t|}{g(t)} > C\right] = 0. \quad (43)$$

Proof. Expanding from the definition of the KL divergence and the variational distributions, we have that:

$$\begin{aligned} t \geq 0, \quad D_{\text{KL}}(q_{u,t} \| q_{f,\phi_t}^*) &= \mathbb{E}_{m \sim q_{u,t}} [\log q_{u,t}(m) - \log q_{f,\phi_t}^*(m)] \\ &= \mathbb{E}_{m \sim q_{u,t}} [u_t(m) - f(m, \phi_t)] \\ &\quad + \log \left(\sum_{m' \in \mathcal{M}} p(m') \exp f(m', \phi_t) \right) - \log \left(\sum_{m' \in \mathcal{M}} p(m') \exp u_t(m') \right). \end{aligned} \quad (44)$$

Under assumptions B.1 and B.2, given any $\beta > 0$, applying standard sub-Gaussian concentration results (4) and a union bound, we have that, for all $t \geq 0$:

$$\begin{aligned} \mathbb{P}[\exists m \in \mathcal{M} : |f(m, \phi_t) - \mu_t(m, \phi_t)| > \beta \sigma_t(m, \phi_t)] &\leq \sum_{m \in \mathcal{M}} \mathbb{P}[|f(m, \phi_t) - \mu_t(m, \phi_t)| > \beta \sigma_t(m, \phi_t)] \\ &\leq 2|\mathcal{M}| \exp\left(-\frac{\beta^2}{2}\right) \\ &=: \delta_\beta. \end{aligned} \quad (45)$$

With probability at least $1 - \delta_\beta$, it then follows that:

$$u_t(m) - f(m, \phi_t) = \mu_t(m, \phi_t) + \beta \sigma_t(m, \phi_t) - f(m, \phi_t) \leq 2\beta \sigma_t(m, \phi_t) \quad (46)$$

$$\log \left(\sum_{m' \in \mathcal{M}} p(m') \exp f(m', \phi_t) \right) - \log \left(\sum_{m' \in \mathcal{M}} p(m') \exp u_t(m') \right) \leq 0 \quad (47)$$

for all $m \in \mathcal{M}$. Hence, with the same probability, it holds that:

$$\forall t \geq 0, \quad D_{\text{KL}}(q_{u,t} || q_{f,\phi_t}^*) \leq 2\beta \mathbb{E}_{m \sim q_{u,t}} [\sigma_t(m, \phi_t)] \leq 2\beta \|\sigma_t(\cdot, \phi_t)\|_\infty. \quad (48)$$

By Lemma B.2, we know that $\sigma_t(m, \phi_t) \in \mathcal{O}(t^{-1/2})$, so that there exists $C > 0$ such that $\sigma_t(m, \phi_t) \leq Ct^{-1/2}$, for all $m \in \mathcal{M}$. We then have that:

$$\begin{aligned} \lim_{\beta \rightarrow \infty} \limsup_{t \rightarrow \infty} \mathbb{P} \left[\frac{D_{\text{KL}}(q_{u,t} || q_{f,\phi_t}^*)}{Ct^{-1/2}} > 2\beta \right] &\leq \lim_{\beta \rightarrow \infty} \limsup_{t \rightarrow \infty} \mathbb{P} [D_{\text{KL}}(q_{u,t} || q_{f,\phi_t}^*) > 2\beta \|\sigma_t(\cdot, \phi_t)\|_\infty] \\ &\leq \lim_{\beta \rightarrow \infty} 2|\mathcal{M}| \exp \left(-\frac{\beta^2}{2} \right) = 0, \end{aligned} \quad (49)$$

which concludes the proof. \square

C Proof of bijective equivalence between discrete distributions

Proof of Proposition 3.1. Let \mathcal{P} denote the set of all finite discrete distributions over \mathcal{M} , and let \mathcal{C} denote the set of categorical distributions parameterized by θ .

Injectivity: Suppose θ and ϕ are two distinct probability vectors in \mathcal{C} . Then, there exists at least one index i such that $\theta_i \neq \phi_i$. Consequently, the corresponding distributions assign different probabilities to m_i , implying $\theta \neq \phi$.

Surjectivity: For any finite discrete distribution $\mathbf{p} \in \mathcal{P}$, define $\theta = \mathbf{p}$. Since \mathbf{p} satisfies $\theta_i \geq 0$ and $\sum_{i=1}^k \theta_i = 1$, θ is a valid parameterization in \mathcal{C} . Thus, every \mathbf{p} corresponds to some θ .

Since the mapping is both injective and surjective, it is bijective. Therefore, every finite discrete distribution has a unique categorical distribution representation. \square

D Monte Carlo gradients via score function estimation

An alternative to the reparameterization trick is the score function estimator (SFE), which circumvents the issue of non-differentiable samples from discrete distributions by using the log trick to compute the gradients of a function with respect to variational parameters. In the case of the distribution of models, we have the identity

$$\nabla_{\psi} q_{\psi}(m) = q_{\psi}(m) \nabla_{\psi} \log q_{\psi}(m). \quad (50)$$

By the Leibniz integral rule, the gradient of the expectation in equation 10 with respect to the parameters of the discrete distribution is

$$\begin{aligned} \nabla_{\psi} \mathcal{L}(\phi, \psi) &= \nabla_{\psi} \mathbb{E}_{m \sim q_{\psi}} [\ell(m)] + \nabla_{\psi} \mathbb{E}_{m \sim q_{\psi}} \left[\log \frac{q_{\psi}(m)}{p(m)} \right] \\ &= \mathbb{E}_{m \sim q_{\psi}} [\ell(m) \nabla_{\psi} \log q_{\psi}(m)] + \mathbb{E}_{m \sim q_{\psi}} \left[\log \frac{q_{\psi}(m)}{p(m)} \nabla_{\psi} \log q_{\psi}(m) \right]. \end{aligned}$$

In practice, the variance of this estimator can be very high when the batch size is not large. However, there are techniques to reduce this variance for general applications. The simplest of which is to use a control variate ς in the form

$$\nabla_{\psi} \mathcal{L}(\phi, \psi) = \mathbb{E}_{m \sim q_{\psi}} [\mathbb{E}_{\mathbf{z} \sim \nu_{d_{\max}}} [h(\psi, \phi, \mathbf{z}) - \varsigma] \nabla_{\psi} \log q_{\psi}(m)]. \quad (51)$$

By simply choosing $\varsigma = \mathbb{E}_{t \in \{1, \dots, T\}} [\mathcal{L}(\phi, \psi)]$, where the expectation is estimated online over the iterations of the optimizer, we can reduce variance of $\nabla_{\psi} \mathcal{L}(\phi, \psi)$. See Appendix D.1 for implementation details.

D.1 Control variate for score function estimator

We adopt the approach used in Kingma and Ba (21) for obtaining an unbiased running first moment of the loss function. At iteration t we draw B samples $\{m_{t,n}\}_{n=1}^B$ and compute

$$\ell_{t,n} = -\hat{\mathcal{L}}_{t,n}, \quad n = 1, \dots, B.$$

With fixed decay $\beta \in (0, 1)$, update the (biased) first moment exactly as in the approach of the Adam optimizer (21):

$$\tilde{\mu}_t \leftarrow \beta \tilde{\mu}_{t-1} + (1 - \beta) \bar{\ell}_t, \quad \bar{\ell}_t = \frac{1}{B} \sum_{n=1}^B \ell_{t,n}.$$

To remove the initialization bias,

$$\mu_t \leftarrow \frac{\tilde{\mu}_t}{1 - \beta^t}.$$

Using $\varsigma_t := \mu_t$ as a baseline, the Monte Carlo gradient estimator becomes

$$\tilde{\nabla}_{\psi,t} \leftarrow \frac{1}{B} \sum_{n=1}^B (\ell_{t,n} - \varsigma_t) \nabla_{\psi} \log q_{\psi}(m_{t,n}).$$

Because ς_t is independent of each $m_{t,n}$, the estimator remains unbiased while the baseline substantially reduces its variance.

D.2 Controlling learning rate via the information gain

When using stochastic gradient descent for optimization over parameters of both q_{ψ} and q_{ϕ} , it is necessary to use careful scaling of the estimated gradients to ensure the optimizer does not “drop off a cliff” into a local minimum. Such phenomena has been observed in related fields such as proximal policy gradients (38) where the authors demonstrate empirically such a necessity in reinforcement learning problems. In essence, we want to control the learning rate of ψ with respect to the convergence of $\phi \rightarrow \phi^*$. We show empirical results for controlling this rate and leave any mathematical properties for the optimal scaling to future research.

One approach is to control the rate of *information gain* (IG) of q_{ψ} during the simultaneous optimization over both ψ and ϕ . By assuming a bounded rate of information gain for q_{ϕ} (achieved via gradient clipping) we only

need to consider computing the IG over successive $q_\psi^{(t)}$ for steps $t = 1, \dots, T$. Defining the IG in terms of entropy, we have

$$\text{IG}(q_\psi^{(t+1)} | q_\psi^{(t)}) = H(q_\psi^{(t)}) - H(q_\psi^{(t+1)}). \quad (52)$$

When q_ψ is a categorical distribution, this quantity is available analytically. However, in general this is not available, but it can be estimated via Monte Carlo integration and importance sampling using available quantities (see Appendix D.3). We choose to set a threshold for the IG between steps, denoted $\beta_{\text{IG}(\psi)}$, and then at each successive step t we scale ∇_ψ using an iterative method such as bisection⁴.

D.3 Monte Carlo estimation of information

The below procedure assumes q_ψ represents a distribution over strings of Bernoulli variables. Let $\psi \in \mathbb{R}^{n_\psi}$ parameterize a masked autoencoder that determines logits for a product Bernoulli distribution

$$q_\psi(m) = \prod_{i=1}^d \sigma(\text{NN}_\psi^{(i)}(m))^{m^{(i)}} [1 - \sigma(\text{NN}_\psi^{(i)}(m))]^{1-m^{(i)}}, \quad m \in \{0, 1\}^d,$$

with MADE logits $\text{NN}_\psi^{(i)}(\cdot)$ and $\sigma(\text{NN}_\psi) = (1 + e^{-\text{NN}_\psi})^{-1}$. After an SGD proposal $\psi' = \psi - \alpha \nabla_\psi$, we estimate the entropy reduction

$$\Delta\mathcal{I}(\alpha) = H(q_\psi) - H(q_{\psi'}), \quad H(p) = -\sum_m p(m) \log p(m). \quad (53)$$

To reduce computation at the expense of introducing some estimation bias, we employ importance weights to re-use the current sample of model indicators in an iterative search to scale the gradient step. Draw a mini-batch $\{m^{(n)}\}_{n=1}^N \stackrel{\text{i.i.d.}}{\sim} q_\psi$ *once*; no re-sampling is needed afterwards. Because the expectation in equation 53 switches from q_ψ to $q_{\psi'}$, rewrite

$$H(q_{\psi'}) = -\mathbb{E}_{m \sim q_\psi} [w_{\psi', \psi}(m) \log q_{\psi'}(m)], \quad w_{\psi', \psi}(m) := \frac{q_{\psi'}(m)}{q_\psi(m)}. \quad (54)$$

For a Bernoulli product the weight factorizes:

$$w_{\psi', \psi}(m) = \prod_{i=1}^d \frac{\sigma(\text{NN}_{\psi'}^{(i)}(m))^{m^{(i)}} [1 - \sigma(\text{NN}_{\psi'}^{(i)}(m))]^{1-m^{(i)}}}{\sigma(\text{NN}_\psi^{(i)}(m))^{m^{(i)}} [1 - \sigma(\text{NN}_\psi^{(i)}(m))]^{1-m^{(i)}}} \quad (\text{NN}_\psi^{(i)} := \text{NN}_\psi^{(i)}(m), \text{NN}_{\psi'}^{(i)} := \text{NN}_{\psi'}^{(i)}(m)), \quad (55)$$

implemented stably via $\frac{\sigma(\text{NN}_{\psi'}^{(i)}(m))}{\sigma(\text{NN}_\psi^{(i)}(m))} = \exp[\log(1 + e^{-\text{NN}_\psi^{(i)}(m)}) - \log(1 + e^{-\text{NN}_{\psi'}^{(i)}(m)})]$.

The mini-batch estimator is therefore

$$\widehat{H}_N(\psi') = -\frac{1}{N} \sum_{n=1}^N w_{\psi', \psi}(m^{(n)}) \log q_{\psi'}(m^{(n)}), \quad \widehat{H}_N(\psi) = -\frac{1}{N} \sum_{n=1}^N \log q_\psi(m^{(n)}). \quad (56)$$

Given a tolerance $\varepsilon > 0$, reduce $\alpha \leftarrow 0.5 \alpha$ until

$$|\widehat{H}_N(\psi) - \widehat{H}_N(\psi')| \leq \varepsilon. \quad (57)$$

If no $\alpha > 10^{-20}$ satisfies equation 57, discard the update by setting the gradient to $\mathbf{0}$. Otherwise, apply the accepted scaled gradient.

⁴In preliminary investigations, other approaches for implementation of this threshold such as constrained optimization and computation of Lagrange multipliers were trialed without success, possibly due to the geometry of the optimization landscape.

E Robust variable selection example details and additional results

The likelihood setup is

$$p(y_i | \mathbf{x}_i, \boldsymbol{\beta}, \boldsymbol{\gamma}) = \boldsymbol{\mu}(\mathbf{x}_i) + (1 - \alpha) \mathcal{N}(y_i; 0, \sigma_1^2) + \alpha \mathcal{N}(y_i; 0, \sigma_2^2), \quad (58)$$

with priors $p(\boldsymbol{\gamma}) = 2^{-p}$ and $p(\boldsymbol{\beta}) = \mathcal{N}(0, \sigma_\beta^2 \mathbf{I})$. Each of the parameters in the likelihood are described in Table 2 under the Misspecification:None column. The data generating setup in Table 2 describes three levels of misspecification to induce poor identifiability and thus a posterior that is challenging to fit using simple variational density families, such as mean field inference. This exemplifies the use of normalizing flows for this experiment. While many parameters are shared, some differ strongly between the likelihood and DGP. In particular, notice the difference in σ_1, σ_2 . Also, for the highly misspecified DGP, correlation between included covariates i and excluded covariates j is induced by a factor of $\rho_{i,j} = 0.1$ for a proportion of j , making the recovery of the DGP using any inference method a challenging and improbable task. For every data set, $\boldsymbol{\beta}$ will be either $\boldsymbol{\beta}_1$ or $\boldsymbol{\beta}_2$ with probability 0.5.

Table 2: Data generating setup

Parameter	Misspecification to likelihood		
	None	Mid	High
Number of data points $ \mathbf{x} $	50		
Dimension of $\boldsymbol{\beta}$	8		
Dimension of $\boldsymbol{\gamma}$	7		
$ \mathcal{M} $	$2^7 = 128$		
Probability of inclusion $\mathbb{P}(\gamma_i = 1)$	0.4		
Non-outlier σ_1	1	2	4
Outlier σ_2	10	5	4
Probability of correlation $\mathbb{P}(\rho_{i,j} > 0 \gamma_i = 1, \gamma_j = 0)$	0		0.4
Total correlation factor $\sum_j \rho_{i,j}$	0		0.1
β_1	0.5		
β_2	0.5	1.5	
Outlier probability α	0.1		

Lastly, during the inference process, we consider two separate experiments for each DGP: a “focused-prior” experiment where $\sigma_\beta = 1.5$, and a “wide-prior” experiment where $\sigma_\beta = 10$. These two scenarios cause a significant difference between the inferred reversible jump MCMC model probabilities and the inferred VTI model probabilities, as can be seen in the subsequent figures.

VTI inference was conducted on a cluster of GPU nodes with mixed Nvidia *RTX3090* and *H100* cards. On the former we used float32 precision for MLP architectures, the latter used float64.

E.1 Sweep of increasing cardinality

Using the focused prior setup on both the medium and high misspecification level targets, we sweep the cardinality of the model space $|\mathcal{M}|$ from $2^9 = 512$ to $2^{24} = 16,777,216$ and compute the cross entropy $H(\pi, q_{\psi, \phi})$. The reversible jump MCMC process in Appendix E.4 was used to obtain gold 1,000 standard samples from the “true” $\pi(m, \boldsymbol{\theta}_m)$, based on 50,000 chain iterations and retaining every 50th sample. The results of 1,024 replicate chains are visualized in Figure 4, which shows how the cross entropy $H(\pi, q_{\psi, \phi})$ changes with $|\mathcal{M}|$. Although $H(\pi, q_{\psi, \phi})$ generally increases with $|\mathcal{M}|$, we notice that, as expected (with the existing tuning parameters), the surrogate method (blue bars) performs comparably with the other methods for the smaller model spaces ($|\mathcal{M}| = 2^9$), whereas the neural density (orange bars) performs consistently as $|\mathcal{M}|$ increases.

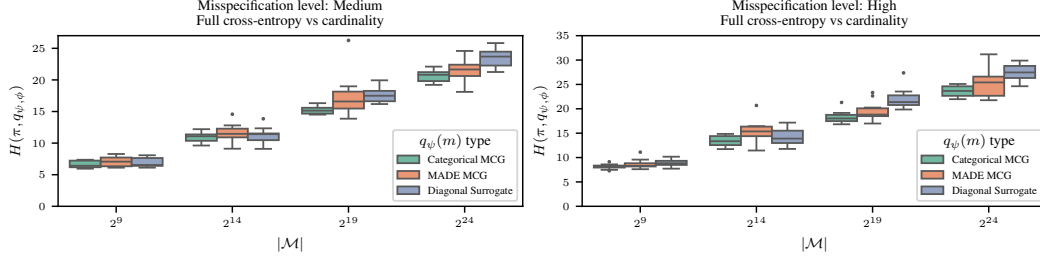


Figure 4: A simulation study showing the cross entropy (NLL) between reversible jump MCMC samples and an amortized variational transdimensional density using rational quadratic spline CoSMIC flows under a fixed number of iterations (30,000). Each cardinality was run with 10 independently sampled synthetic data sets.

E.2 Focused versus wide priors

Each of Figures 5–10 is a replicate of Figure 2 in the main text, showing a sweep of 10 randomly generated data sets (indicated by different colours) according to the corresponding setup in Table 2 using three different variational families: diagonal Gaussian MLP (a CoSMIC mean-field variational family), a composition of 5 affine masked autoregressive flows each with 5 hidden blocks, and a composition of 4 rational quadratic spline masked autoregressive flows each with 6 hidden blocks. The expressiveness of each variational family increases from left to right in each figure.

In the $\sigma_\beta = 1.5$ focused prior setting (Figures 5, 7, 9) performance is generally good, as per Figure 2 in the main text: (i) the model probability estimates (top row) tend to move closer to the $y = x$ line as the expressiveness of the variational family increases (left to right plots); (ii) the slight S-shape of the model probability estimates around the $y = x$ line is easily interpretable as the the variational objective $\mathcal{L}(\psi, \phi)$ (equation 10) will naturally favour models with higher posterior model probability over those with lower probabilities; (iii) the true data generating process models (triangles) are generally given high posterior model probabilities; and (iv) individual model posteriors are better estimated for higher probability models (negative slope on the bottom rows).

For the $\sigma_\beta = 10$ wide prior setting (Figures 6, 8, 10) performance at first glance appears much worse, particularly in terms of estimating model probabilities. However, on closer inspection this is not the case. It is well known (e.g. (14)) that the marginal likelihood (a.k.a. model evidence; a component of the posterior model probability) can be highly sensitive to diffuse priors. In such cases (as with $\sigma_\beta = 10$) the posterior will tend to unreasonably favour those models with fewer parameters, and particularly (in the case of regression models) the null model with no predictors, even in the presence of a very clear relationship between predictors and response. This effect can be clearly seen in Figures 6, 8, 10 (top row), where the null model (indicated by a circle) is given far higher posterior model probability on the $\pi(m)$ axis than the actual data generating process (triangles). In contrast, the true data generating process (triangles) is generally given a high posterior model probability (comparable with the focused prior setting in Figures 5, 7, 9) under the VTI approximation. From these results we conclude that: (i) the posterior model probabilities that depend on the marginal likelihood (i.e., the estimates of $\pi(m)$ on the x -axis) have been affected by the wide prior to unreasonably favour models with less parameters; (ii) the VTI-based posterior model probability estimates suggest that they are less sensitive to the undesirable effects of this prior; and (iii) in combination the resulting plots in Figures 6, 8, 10 (top row) only appear to indicate worse performance of VTI compared to the gold standard than is actually the case.

E.3 Within model comparison

Figure 11 illustrates a typical comparison between the reversible jump MCMC estimated posterior distribution and the VTI approximation. The figure shows the posterior of the data generating process model from the first high misspecification dataset in Figure 2 (main text). While there are some small differences, the main features of the posterior appear to be well captured.

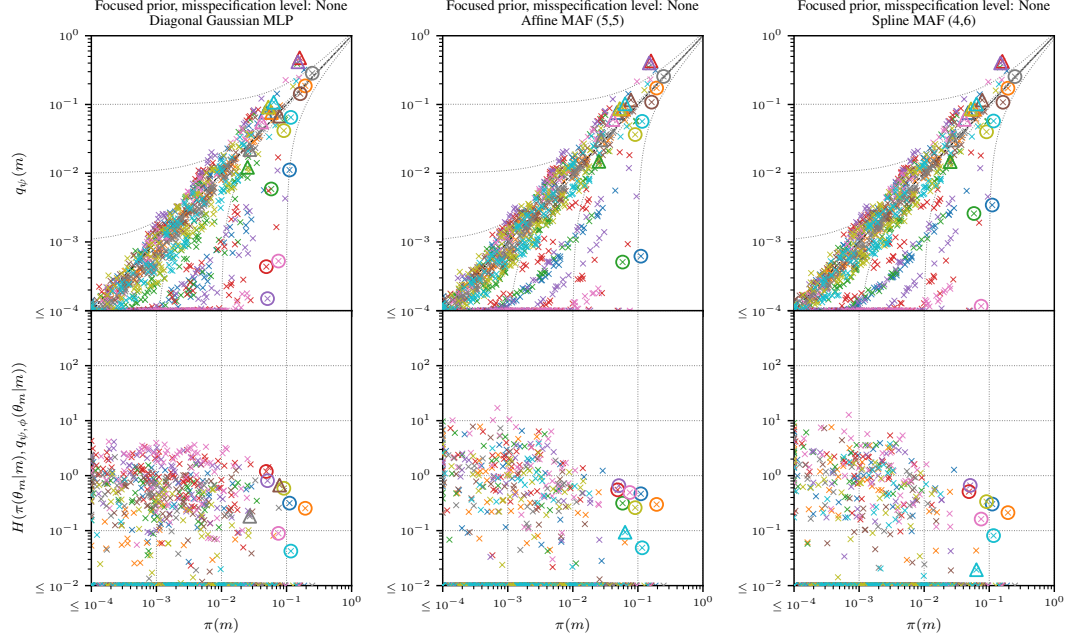


Figure 5: As Figure 2 (main text), but under: *no misspecification* ($\sigma_1 = 1, \sigma_2 = 10$), *focused prior* ($\sigma_\beta = 1.5$). Circles indicate the null model (constant only, no predictors); triangles indicate the data generating process.

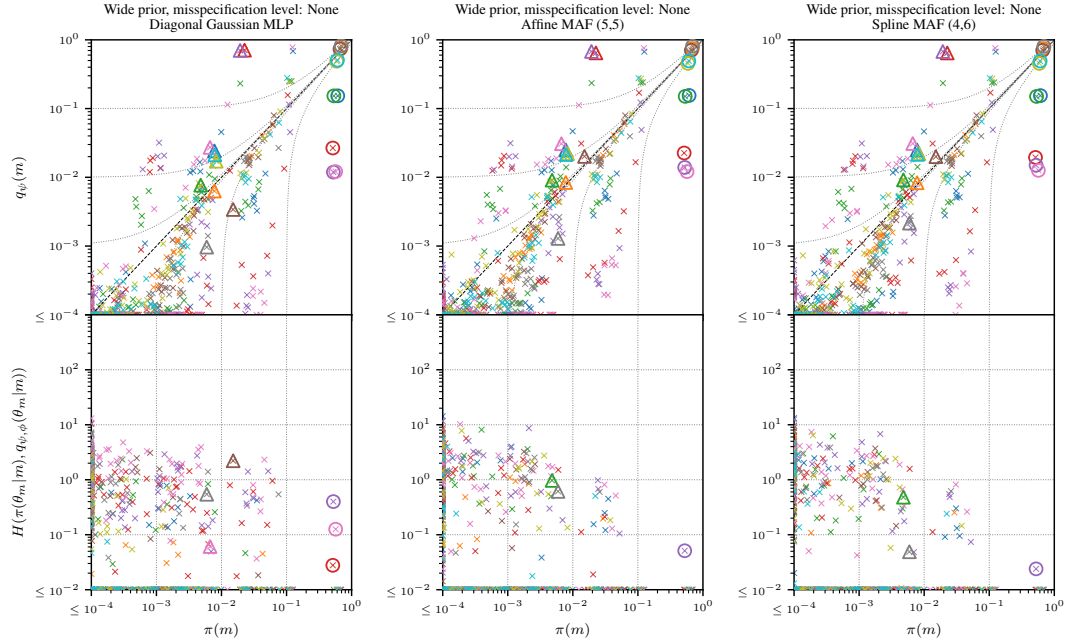


Figure 6: As Figure 2 (main text), but under: *no misspecification* ($\sigma_1 = 1, \sigma_2 = 10$), *wide prior* ($\sigma_\beta = 10$). Circles indicate the null model (constant only, no predictors); triangles indicate the data generating process.

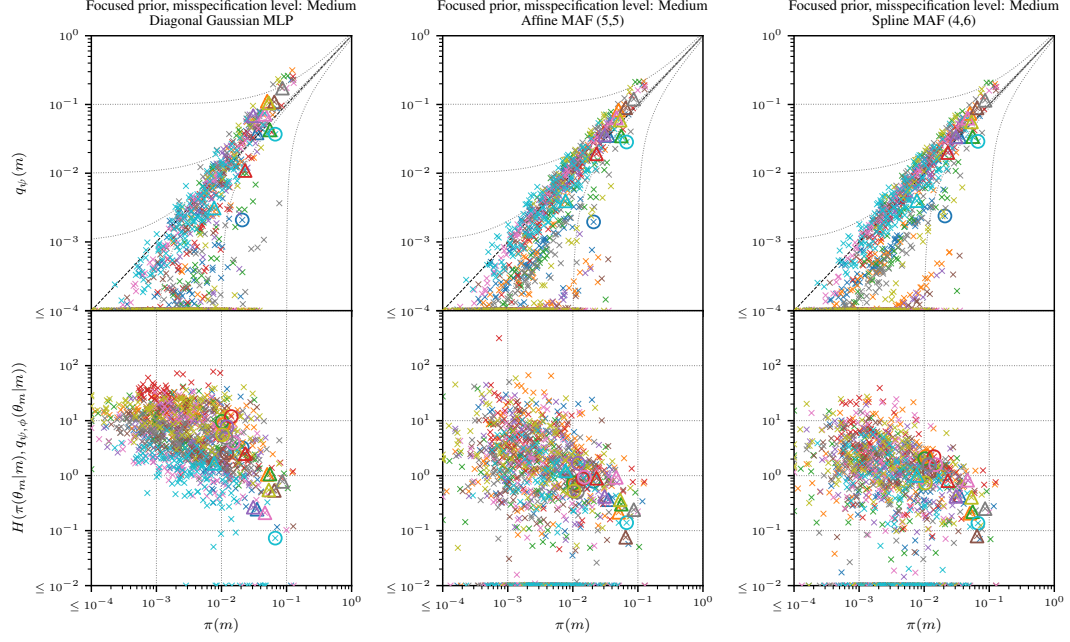


Figure 7: As Figure 2 (main text), but under: *mid misspecification* ($\sigma_1 = 2, \sigma_2 = 5$), *focused prior* ($\sigma_\beta = 1.5$). Circles indicate the null model (constant only, no predictors); triangles indicate the data generating process.

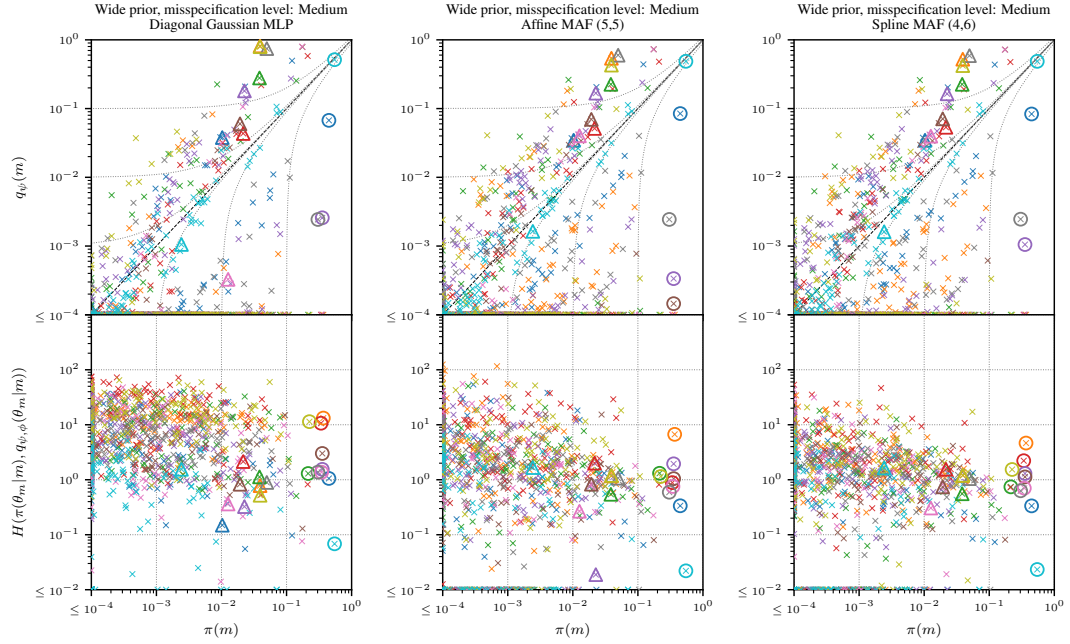


Figure 8: As Figure 2 (main text), but under: *mid misspecification* ($\sigma_1 = 2, \sigma_2 = 5$), *wide prior* ($\sigma_\beta = 10$). Circles indicate the null model (constant only, no predictors); triangles indicate the data generating process.

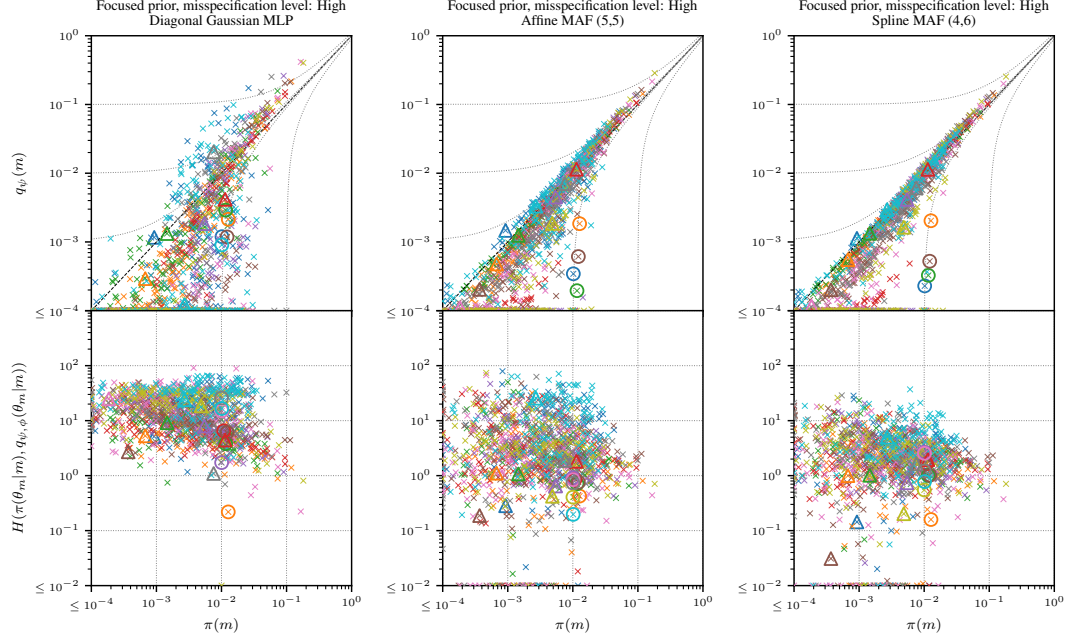


Figure 9: As Figure 2 (main text), but under: *high misspecification* ($\sigma_1 = 4, \sigma_2 = 4$), *focused prior* ($\sigma_\beta = 1.5$). Circles indicate the null model (constant only, no predictors); triangles indicate the data generating process.

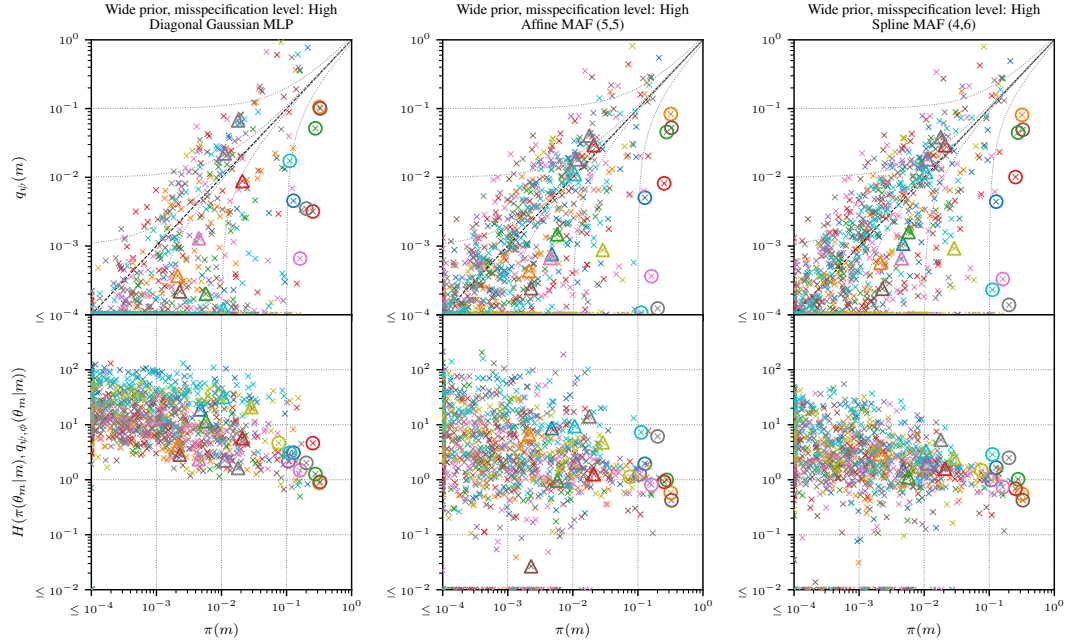


Figure 10: As Figure 2 (main text), but under: *high misspecification* ($\sigma_1 = 4, \sigma_2 = 4$), *wide prior* ($\sigma_\beta = 10$). Circles indicate the null model (constant only, no predictors); triangles indicate the data generating process.

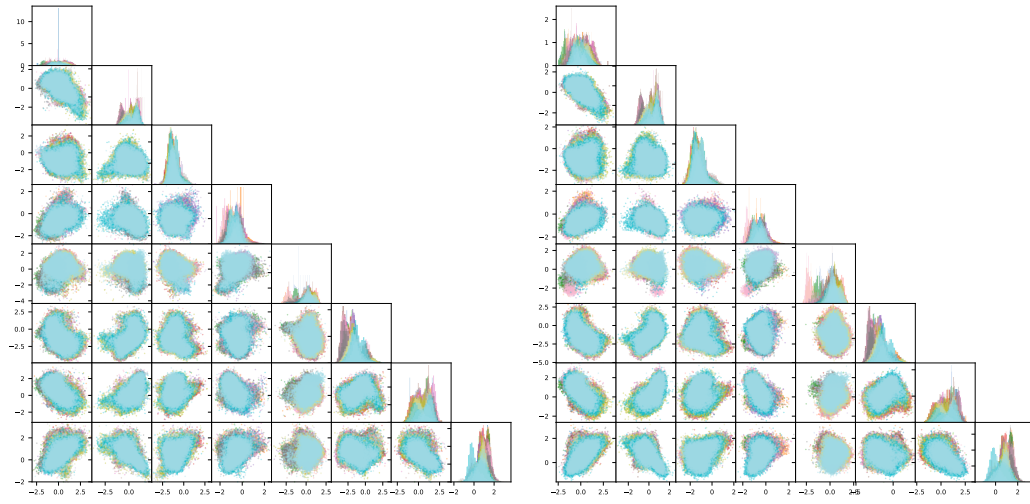


Figure 11: Bivariate plot comparison between reversible jump MCMC (left) and VTI (right) using spline flow composition of four layers and six blocks on the first synthetic high-misspecification data set from the Figure 2 (main text) example.

E.4 Reversible jump MCMC for robust variable selection

Consider the linear model $y = X\beta + \varepsilon$ with $\varepsilon \sim \mathcal{N}(0, \sigma^2 I)$. We introduce a binary mask $m \in \{0, 1\}^p$ to indicate active coefficients in $\beta \in \mathbb{R}^p$. The reversible jump MCMC algorithm explores the model space by proposing bit-flips in m , corresponding to adding (birth) or removing (death) predictors.

Birth Move $(m, \beta) \rightarrow (m', \beta)$: A birth move flips a bit from 0 to 1. The acceptance ratio is derived as follows:

$$\alpha_{\text{birth}} = \min \left\{ 1, \frac{p(y \mid \beta, m') p(\beta \mid m') \pi(m')}{p(y \mid \beta, m) p(\beta \mid m) \pi(m)} \right\}$$

Death Move $(m, \beta) \rightarrow (m', \beta)$:

A death move flips a bit from 1 to 0. The acceptance ratio is the reciprocal of the birth ratio $\alpha_{\text{death}} = \frac{1}{\alpha_{\text{birth}}}$.

Jacobian Determinant: For bit-flipping moves in a saturated space where the dimensionality remains constant ($\dim(m') = \dim(m)$), the transformation is bijective with a Jacobian determinant of 1:

$$\left| \frac{\partial(m', \beta')}{\partial(m, \beta)} \right| = 1.$$

Thus, the Jacobian does not affect the acceptance ratio.

Within-Model Gaussian Proposal $\beta \rightarrow \beta'$: Within a fixed model m , propose a new β' using a symmetric random-walk:

$$\alpha_{\text{within}} = \min \left\{ 1, \frac{p(y \mid \beta', m) p(\beta' \mid m)}{p(y \mid \beta, m) p(\beta \mid m)} \right\}$$

Since the proposal is symmetric, the proposal densities cancel out in the acceptance ratio.

F Example description: Bayesian inference of multi-layer-perceptron directed acyclic graph discovery

Notation:

$\mathbf{X} \in \mathbb{R}^{N_d \times n}$	(columns are i.i.d. samples)
$\mathbf{P} \in \mathcal{P}_{N_d}$	permutation matrix (node order)
$\mathbf{U} \in \{0, 1\}^{N_d \times N_d}$	strictly upper-triangular edge mask
$\mathbf{A} = \mathbf{P}^\top \mathbf{U} \mathbf{P}$	adjacency in canonical order (code default)
$\text{pa}_{\mathbf{A}}(j) = \{i < j : \mathbf{U}_{ij} = 1\}$	parents of node j in the sorted order.

Node-wise conditional mean: Fix hidden width H and a model indicator $m = (\mathbf{P}, \mathbf{U})$. For each *non-root* node $j = 2, \dots, N_d$ define parameters

$$\boldsymbol{\theta}^{(j)} = (W_j^{(1)}, b_j^{(1)}, W_j^{(2)}, b_j^{(2)}) \in \mathbb{R}^{(j+2)H+1},$$

with $W_j^{(1)} \in \mathbb{R}^{H \times (j-1)}$, $b_j^{(1)} \in \mathbb{R}^H$, $W_j^{(2)} \in \mathbb{R}^{1 \times H}$, $b_j^{(2)} \in \mathbb{R}$. Let $\mathbf{u}_j := \mathbf{U}_{1:(j-1), j}$ be the $(j-1)$ -vector of active parents. For $\mathbf{x} = (x_1, \dots, x_{j-1})^\top$,

$$f_j(\mathbf{x}; \boldsymbol{\theta}^{(j)}, \mathbf{U}) = W_j^{(2)} \text{ReLU}(W_j^{(1)}(\mathbf{x} \odot \mathbf{u}_j) + b_j^{(1)}) + b_j^{(2)}, \quad f_1(\cdot) \equiv 0.$$

Gaussian likelihood: Let ϖ be the permutation associated with \mathbf{P} (so $x_{\varpi(j)}$ is column j after sorting). With homoscedastic noise σ^2 ,

$$\log p(\mathbf{X} | \mathbf{P}, \mathbf{U}, \boldsymbol{\theta}) = -\frac{nN_d}{2} \log(2\pi\sigma^2) - \frac{1}{2\sigma^2} \sum_{s=1}^n \sum_{j=1}^{N_d} \left(x_{\varpi(j)}^{(s)} - f_j(\mathbf{x}_{\varpi(1:j-1)}^{(s)}; \boldsymbol{\theta}^{(j)}, \mathbf{U}) \right)^2$$

Parameter prior (masked i.i.d. Gaussian): Let $C(m) \subseteq \{1, \dots, \dim \boldsymbol{\theta}\}$ be the index set that survives the mask. Then

$$p(\boldsymbol{\theta} | \mathbf{P}, \mathbf{U}) = \prod_{k \in C(m)} \mathcal{N}(\boldsymbol{\theta}_k; 0, \sigma_0^2)$$

(parameters outside $C(m)$ are handled by a reference density).

Structural prior:

$$p(\mathbf{P}, \mathbf{U}) \propto \exp(-\lambda \|\mathbf{U}\|_1), \quad \lambda \geq 0,$$

with \mathbf{P} a permutation matrix and \mathbf{U} strictly upper triangular.

The un-normalised log-posterior is the sum of the three boxed terms above.

F.1 Data generating process

The data generating procedure generally follows the simulation design in Thompson et al. (44).

Global hyper-parameters:

N_d : number of nodes, H : hidden width, σ^2 : noise variance,
 $\rho_{\text{Edge}} \in (0, 1)$: edge probability, $\sigma_0 > 0$: parameter prior scale.

Sample graph structure:

$$\begin{aligned} \mathbf{P} &\sim \text{Uniform}(\mathcal{P}_{N_d}), \\ \mathbf{U}_{ij} &\stackrel{\text{iid}}{\sim} \text{Bernoulli}(\rho_{\text{Edge}}), \quad 1 \leq i < j \leq N_d, \\ \mathbf{A} &= \mathbf{P}^\top \mathbf{U} \mathbf{P}. \end{aligned}$$

Sample node parameters: Let the *bias flag* $\beta \in \{0, 1\}$ ($\beta = 1$ keeps both bias vectors, $\beta = 0$ sets them to 0). For each non-root node $j = 2, \dots, N_d$ draw independently

$$\boldsymbol{\theta}^{(j)} = (W_j^{(1)}, \beta b_j^{(1)}, W_j^{(2)}, \beta b_j^{(2)}), \quad [\boldsymbol{\theta}^{(j)}]_k \stackrel{\text{iid}}{\sim} [-0.7, -0.3] \cup [0.3, 0.7],$$

while the root node has $\boldsymbol{\theta}^{(1)} = \emptyset$. Note the active parameters are drawn uniformly from a non-zero range rather than from the prior.

Context-to-mask map: For $m = (\mathbf{P}, \mathbf{U})$, $C(m) = C(\mathbf{U}) \subseteq \{1, \dots, \dim \boldsymbol{\theta}\}$ keeps exactly the coordinates satisfying the conditions:

1. Column i of $W_j^{(1)}$ is *active* iff $U_{ij} = 1$;
2. If $\sum_{i < j} U_{ij} = 0$ then *all* parameters in $\boldsymbol{\theta}^{(j)}$ are masked.

(The permutation \mathbf{P} has no effect on the mask.)

Data generation (topological order): Let ϖ be the permutation induced by \mathbf{P} . For each sample $s = 1, \dots, n$ generate sequentially

$$\begin{aligned} x_{\varpi(1)}^{(s)} &= \sigma \varepsilon_{1s}, \\ x_{\varpi(j)}^{(s)} &= f_j(\mathbf{x}_{\varpi(1:j-1)}^{(s)}; \boldsymbol{\theta}^{(j)}, \mathbf{U}) + \sigma \varepsilon_{js}, \quad j = 2, \dots, N_d, \end{aligned}$$

where $\varepsilon_{js} \stackrel{\text{iid}}{\sim} \mathcal{N}(0, 1)$ and

$$f_j(\mathbf{z}; \boldsymbol{\theta}^{(j)}, \mathbf{U}) = W_j^{(2)} \text{ReLU}(W_j^{(1)}(\mathbf{z} \odot \mathbf{u}_j) + \beta b_j^{(1)}) + \beta b_j^{(2)}, \quad \mathbf{u}_j := \mathbf{U}_{1:(j-1), j}.$$

Collecting the n draws gives

$$\mathbf{X} = \begin{bmatrix} \mathbf{x}^{(1)} \\ \vdots \\ \mathbf{x}^{(n)} \end{bmatrix} \in \mathbb{R}^{n \times N_d}, \quad \text{stored in topological order } (x_{\varpi(1)}, \dots, x_{\varpi(N_d)}).$$

F.2 Comparison metrics

Given knowledge of a “true” adjacency matrix A , each experiment uses four scores for comparison with the estimated posterior: F1, structured Hamming distance (SHD), Brier score, and area under the receiver operating characteristic curve (AUROC). This follows the experiment setup in Thompson et al. (44).

F.3 Common inference setup

For each data set in both the simulation study and real data example, VTI is run a total of 10 replicates using different random seeds, and the posterior is selected where the terminal loss is minimized. For DAGMA, the sparsity hyperparameter is swept from $\lambda^{\min} = 10^{-3}$ to $\lambda^{\max} = 1$ over 10 logarithmically spaced values. For the autoregressive flow, we use Affine(5,5) (see Appendix A.2) with a context encoder designed as follows:

$$\delta(\mathbf{P}, \mathbf{U}) = \sigma^{\lceil \times 2 \rceil} \circ \dots \circ \sigma^{\lceil \times 2 \rceil} \circ (\mathbf{P}^\top \mathbf{U} \mathbf{P}),$$

where $\sigma^{\lceil \times 2 \rceil}(x) := Wx + b$ broadcasts from $|x|$ to the first power of 2 greater than or equal to $2|x|$. The final dimension of $\delta(\mathbf{P}, \mathbf{U})$ is 4096.

F.4 Simulation design

In the simulation study, the configuration of the MLP is as follows. We set the hidden layer width to $H = 10$. We set the number of nodes to $N_d = 10$. We omit the bias parameters $b_j^{(1)}, b_j^{(2)}$ for all edges, i.e. set $\beta = 0$. The edge inclusion probability is set to $\rho_{\text{Edge}} = 0.5$. For VTI, the model prior $p(m)$ is uniform (i.e. the sparsity parameter is set to $\lambda = 0$).

We generate 10 i.i.d. complete data sets of length $n_{\max} = 2^{10}$ from the above process. The experiment compares data size against the metrics from Appendix F.2. The range of data sizes are $n = 16, 32, 4, 128, 256, 512, 1024$, where $n < n_{\max}$ simply takes the first n samples.

VTI inference was conducted on a cluster of GPU nodes with mixed Nvidia *RTX3090* and *H100* cards. On the former we used float32 precision for MLP architectures, the latter used float64.

F.5 Real data example

For VTI, we chose a penalized structural model prior $p(m)$ where $\lambda = 200$. We set the number of hidden nodes per edge to $H = 5$ and include the bias terms, i.e. $\beta = 1$.

For DAGMA non-linear, we use 10 hidden nodes per edge and no bias term.

F.6 DAG Model indicator construction: Lehmer Code Decoding

A permutation of the ordered set $\{1, 2, \dots, N_d\}$ is represented by a *Lehmer code* $\mathbf{c} = (c_1, c_2, \dots, c_{N_d})$, where $c_i \in \{0, 1, \dots, N_d - i\}$. At step i ($1 \leq i \leq N_d$) we choose the $(c_i + 1)$ -th *unused* index in the remaining ascending list.

Example. For $N_d = 5$ and $\mathbf{c} = (2, 1, 0, 0, 0)$

$$\begin{aligned} c_1 = 2 : & \{1, 2, 3, 4, 5\} \rightarrow 3, \\ c_2 = 1 : & \{1, 2, 4, 5\} \rightarrow 2, \\ c_3 = 0 : & \{1, 4, 5\} \rightarrow 1, \\ c_4 = 0 : & \{4, 5\} \rightarrow 4, \\ c_5 = 0 : & \{5\} \rightarrow 5. \end{aligned}$$

Permutation-matrix representation. The permutation ϖ is stored as a one-hot $\mathbf{P} \in \{0, 1\}^{N_d \times N_d}$ with $P_{r,i} = 1$ iff row r is chosen at column i .

Algorithm 2 Vectorized Lehmer decode via leftover mask

Require: $P_{\text{code}} \in \mathbb{N}^{B \times N_d}$ {batch of Lehmer codes}
Ensure: $\mathbf{P} \in \{0, 1\}^{B \times N_d \times N_d}$

- 1: $\text{bs} \leftarrow B$
- 2: $\mathbf{P} \leftarrow \mathbf{0}_{\text{bs} \times N_d \times N_d}$
- 3: **for** $i = 1$ **to** $N_d - 1$ **do**
- 4: $k \leftarrow P_{\text{code}}[:, i]$
- 5: $\text{OneHot} \leftarrow \text{one_hot}(k, N_d - i + 1)$ {shape = $\text{bs} \times (N_d - i + 1)$ }
- 6: $\text{Used} \leftarrow \sum_{c=1}^{i-1} \mathbf{P}[:, :, c]$
- 7: $\text{Mask} \leftarrow (\text{Used} = 0)$
- 8: $\text{Idx} \leftarrow \text{nonzero}(\text{Mask})$
- 9: $\mathbf{P}[\text{Idx}[:, 0], \text{Idx}[:, 1], i] \leftarrow \text{reshape}(\text{OneHot}, -1)$
- 10: **end for**
- 11: $\text{Used} \leftarrow \sum_{c=1}^{N_d-1} \mathbf{P}[:, :, c]$
- 12: $\text{Last} \leftarrow \text{nonzero}(\text{Used} = 0)$
- 13: $\mathbf{P}[\text{Last}[:, 0], \text{Last}[:, 1], N_d] \leftarrow 1$
- 14: **return** \mathbf{P}

Algorithm 2 decodes each column in parallel. For column i the code $k \in [0, N_d - i]$ specifies “pick the $(k+1)$ -th leftover row.” The Boolean mask marks currently unused rows; broadcasting the flattened one-hot vector onto the corresponding (batch, row) pairs writes the unit entries. Column N_d is filled by the single row that remains

unassigned. This implementation gives a compact (B, N_d) tensor, expanded by the decoder to (B, N_d, N_d) for efficient batched linear algebra in our DAG-inference pipeline.

F.7 Model identifier for directed acyclic graphs

We encode a permutation matrix $\mathbf{P} \in \{0, 1\}^{N_d \times N_d}$ using a *compressed Lehmer code* consisting of $N_d - 1$ categorical variables $\{\rho_1^{\text{cat}}, \dots, \rho_{N_d-1}^{\text{cat}}\}$. Here ρ_i^{cat} has $N_d - i + 1$ outcomes.

Concretely, $\rho_1^{\text{cat}} \in \{0, 1, \dots, N_d - 1\}$, $\rho_2^{\text{cat}} \in \{0, 1, \dots, N_d - 2\}$, \dots , $\rho_{N_d-1}^{\text{cat}} \in \{0, 1\}$. Once the first $N_d - 1$ columns are fixed, the last column is forced.

Each $\rho_i^{\text{cat}} = k$ is mapped to a one-hot vector of length N_d . The value k selects the $(k+1)$ -st *available* row for the i -th column; previously taken rows remain zero, preserving the permutation property.

Given \mathbf{P} we form an upper-triangular mask $\mathbf{U} \in \{0, 1\}^{N_d \times N_d}$ with zero diagonal. Each entry above the diagonal ($i < j$) is a Bernoulli variable, so \mathbf{U} flattens to $\frac{N_d(N_d-1)}{2}$ bits. The adjacency matrix is $\mathbf{A} = \mathbf{P}^\top \mathbf{U} \mathbf{P}$, giving a DAG.

We concatenate the $N_d - 1$ categorical codes with the $\frac{N_d(N_d-1)}{2}$ Bernoulli bits, yielding a vector \mathbf{z} of length $(N_d - 1) + \frac{N_d(N_d-1)}{2}$. MADE⁺ consumes \mathbf{z} together with a multiplier_fn specifying the parameter count for each entry.

Let z_j denote the j -th component of \mathbf{z} :

$$\text{multiplier_fn}(j) = \begin{cases} N_d - j, & j = 1, \dots, N_d - 1, \\ 1, & j = N_d, \dots, N_d - 1 + \frac{N_d(N_d-1)}{2}. \end{cases}$$

The architecture yields the autoregressive factorization

$$p(\mathbf{z}) = \prod_{j=1}^{N_d-1 + \frac{N_d(N_d-1)}{2}} p(z_j \mid z_{<j}).$$

The identifier $\{\rho_1^{\text{cat}}, \dots, \rho_{N_d-1}^{\text{cat}}, \mathbf{U}_{\text{binary}}\}$ is modelled autoregressively by a single MADE⁺ network, yielding $\mathbf{A} = \mathbf{P}^\top \mathbf{U} \mathbf{P}$ upon sampling.

We employ a structural prior over the space of models with the edge-penalty term γ :

$$p(\mathbf{P}, \mathbf{U} \mid \gamma) = \frac{1}{N_d!} \frac{1}{2^{\frac{N_d(N_d-1)}{2}}} \exp(-\gamma \text{nEdges}(\mathbf{U})), \quad (59)$$

$$\text{nEdges}(\mathbf{U}) = \sum_{i < j} U_{ij}, \quad (60)$$

$$\log p = -\log(N_d!) - \frac{N_d(N_d-1)}{2} \log 2 - \gamma \text{nEdges}(\mathbf{U}). \quad (61)$$

Note that when $\gamma = 0$, the prior is uniform.

F.8 Neural probability mass function for model indicators over large spaces: MADE⁺

To represent a distribution over binary strings, we use the Masked Autoencoder for Density Estimation (MADE) (15) implementation found in the Durkan et al. (12) repository. To represent a more complex discrete distribution such as that required by the \mathbf{P}, \mathbf{U} representation of a directed acyclic graph, we apply a simple extension to this architecture to allow us to vary the output dimension multiplier. For presentational clarity we call this extension MADE⁺. The key change in MADE⁺ is the introduction of a per-dimension output multiplier function $r(i)$ that determines how many parameters are emitted for the i -th input dimension in the autoregressive factorization.

In the original MADE, all features share a common multiplier k , yielding an output dimensionality of $k \times d$ when there are d input features. Mathematically, if $\mathbf{x} \in \mathbb{R}^d$, the network outputs $(h_1, h_2, \dots, h_{kd}) \in \mathbb{R}^{kd}$.

In MADE^+ , a function $r : \{0, 1, \dots, d-1\} \rightarrow \mathbb{N}$ is provided, and the final output dimension is $\sum_{i=0}^{d-1} r(i)$. For each input dimension x_i , the network outputs $r(i)$ parameters. Concretely, where d is the number of input features, the final output dimension becomes $\text{total_out_features} = \sum_{i=0}^{d-1} r(i)$. In other words, each input x_i can be associated with a custom number of distributional parameters (e.g., to handle discrete variables of different cardinalities). The masking logic is preserved by replicating each degree, $\deg(x_i)$, exactly $r(i)$ times in the final layer.

Below is a simplified, side-by-side pseudocode comparing MADE (left) and MADE^+ (right). Changes in MADE^+ are highlighted in green.

Algorithm 3 Original MADE
(Final Layer Construction)

```

out_features = features * output_multiplier
final_layer = MaskedLinear(
    in_degrees = prev_out_degrees,
    out_features = out_features,
    autoregressive_features = features,
    is_output = True
)

```

Algorithm 4 MADE^+
(Final Layer Construction)

```

total_out_features =  $\sum_{i=0}^{\text{features}-1} r(i)$ 
final_layer = MaskedLinear(
    in_degrees = prev_out_degrees,
    out_features = total_out_features,
    autoregressive_features = features,
    is_output = True,
    output_multiplier_fn =  $r(i)$ 
)

```

By allowing each input dimension X_i to have its own output multiplier $r(i)$, the MADE^+ architecture provides a more flexible autoregressive decomposition:

$$p(\mathbf{x}) = \prod_{i=1}^d p(x_i \mid x_1, \dots, x_{i-1}),$$

where now the conditional distribution for x_i can be parameterized by $r(i)$ parameters (e.g., logits for a categorical variable of size $r(i)$, or a mean/variance pair, etc.).

Hence, one can naturally combine discrete variables of varying dimensions such as Bernoulli and categorical variables. For example, if x_1 is categorical with 10 categories and x_2 is a Bernoulli variable, one can specify $r(0) = 10$ and $r(1) = 1$, so that the overall conditional densities (or probability mass functions) multiply to form a richer joint model adapting precisely to each variable's nature.